

Peak Alpine metamorphic conditions from staurolite-bearing metapelites in the Monte Rosa nappe (Central European Alps) and geodynamic implications

Joshua D. Vaughan-Hammon¹  | Cindy Luisier^{1,2} | Lukas P. Baumgartner¹ | Stefan M. Schmalholz¹

¹Institute of Earth Sciences, University of Lausanne, Lausanne, Switzerland

²Université de Rennes, CNRS, Géosciences Rennes UMR 6118, Rennes, France

Correspondence

Joshua D. Vaughan-Hammon, Institute of Earth Sciences, University of Lausanne, Lausanne 1015, Switzerland.
Email: Joshua.vaughan-hammon@unil.ch

Funding information

Schweizerischer Nationalfonds zur Förderung der Wissenschaftlichen Forschung, Grant/Award Number: 200021-165756

Abstract

The tectono-metamorphic evolution of the European Alps is still contentious. The Monte Rosa tectonic unit is a prominent nappe in the Central European Alps and estimates of its peak Alpine pressure (P) and temperature (T) conditions are essential for reconstructing its tectono-metamorphic evolution. However, the reported peak Alpine pressure and temperature estimates vary considerably between 1.2 and 2.7 GPa and 490 and 640°C for a variety of lithologies. Here, we show petrology and pseudosection modelling of metapelitic assemblages from the western portions of the Monte Rosa nappe (upper Ayas valley, Italy). We present newly discovered staurolite–chloritoid-bearing metapelitic assemblages. These assemblages exhibit an Alpine high-*P* metamorphic overprint of a former contact-metamorphic mineral assemblage generated by post-Variscan granitic intrusions. Staurolite contains major amounts of Zn (up to 1.0 atoms per formula units), which is currently, in contrast to Fe- and Mg-staurolite end-members, not considered in any thermodynamic database. We employ two end-member mixing models for Zn in staurolite, site mixing, and molecular mixing. Both models enlarge the pressure and temperature stability range for the observed assemblage, where site mixing has the largest influence of ± 0.2 GPa and $\pm 20^\circ\text{C}$. Our results for three metapelite assemblages, with and without staurolite, indicate peak Alpine pressure of 1.6 ± 0.2 GPa and peak temperature of $585 \pm 20^\circ\text{C}$. These peak pressure estimates agree with previously published estimates for metagranites in the nappe, and are in stark contrast with peak pressure obtained from talc-, chloritoid-, phengite-, and quartz-bearing lithologies termed ‘whiteschists’ (>2.2 GPa). Our results confirm a variation of peak Alpine pressure of 0.6 ± 0.2 GPa between metagranite/metapelite lithologies and a nearby whiteschist lens (>2.2 GPa) within the metagranite. Field observations indicate that the studied region is structurally coherent and that the whiteschist is not a tectonic slice formed by tectonic mélange. We suggest that the consistent peak pressure for metapelite and metagranite assemblages represents the regional peak pressure and that the higher pressure recorded in the whiteschist lens is likely due to dynamic pressure, possibly

This is an open access article under the terms of the Creative Commons Attribution-NonCommercial-NoDerivs License, which permits use and distribution in any medium, provided the original work is properly cited, the use is non-commercial and no modifications or adaptations are made.

© 2021 The Authors. *Journal of Metamorphic Geology* published by John Wiley & Sons Ltd.

resulting from tectonic and/or reaction-induced stresses. If the calculated pressure of 1.6 ± 0.2 GPa represents regional peak Alpine conditions, then the Monte Rosa nappe was exhumed from a significantly shallower depth than previously assumed, based on peak pressure estimates > 2.2 GPa for whiteschist lithologies.

KEYWORDS

Central European Alps, high-*P* metamorphism, metapelite, tectonic pressure, Zn-stauroilite

1 | INTRODUCTION

The Western and Central European Alps (Figure 1) played a significant role in the pioneering discoveries of high- and ultra high pressure, UHP, metamorphic rocks (Chopin, 1987; Chopin et al., 1991; Chopin & Monié, 1984; Goffe & Chopin, 1986; Reinecke, 1991). These rocks contain evidence of the geodynamic environment of orogens and provide insight into pressures, temperatures, and chemical systems unobservable to humans. Geographically, the Monte Rosa nappe is located in the Central European Alps. It is a continental unit belonging to the Middle Penninic domain generated during the western Alpine orogeny (Figure 1; e.g. Handy et al., 2010), that underwent HP conditions associated with its burial below the Adriatic continent during the orogenesis. Petrological investigations into rare magnesiochloritoid-bearing lithologies (named ‘whiteschists’) revealed Alpine eclogite facies metamorphic conditions (Chopin & Monié, 1984). These discoveries prompted numerous studies assessing suitable mechanisms by which UHP crustal rocks can be transported during orogenesis to and from significant depth; sometimes more than 100 km if lithostatic pressure is assumed (Hacker & Gerya, 2013; Kurz & Froitzheim, 2002). However, published estimates of peak Alpine metamorphic conditions for the Monte Rosa nappe highlight large disparities; with peak pressure estimates ranging between 1.2 and 2.7 GPa and temperature (*T*) estimates between 490 and 640°C (Figure 2a; Borghi et al., 1996; Chopin & Monié, 1984; Dal Piaz & Lombardo, 1986; Ferrando et al., 2002; Gasco et al., 2011; Keller et al., 2004; Lapen et al., 2007; Le Bayon et al., 2006; Luisier et al., 2019).

The assessment of suitable mechanisms by which rocks can be transported through an orogen from UHP conditions to the surface requires an estimate of the maximal burial depth at which they equilibrated (e.g. Petrini & Podladchikov, 2000). Large disparities in peak pressure within a structurally coherent nappe poses difficulties when attempting to resolve the tectono-metamorphic history if it is assumed that peak pressure represents the lithostatic pressure, which is mainly a function of burial depth (Schenker et al., 2015; Schmalholz & Podladchikov, 2014). However, the pressure, or mean stress, in a rock

cannot be exactly lithostatic during an orogeny due to differential stresses, required to drive rock deformation (Gerya, 2015; Mancktelow, 1993, 1995, 2008; Schmalholz & Podladchikov, 2013) or to balance lateral variations in gravitational potential energy (Molnar & Lyon-Caen, 1988; Schmalholz et al., 2014, 2019). The deviation from lithostatic pressure is commonly termed tectonic pressure and both its magnitude (Li et al., 2010; Luisier et al., 2019; Reuber et al., 2016) and impact on metamorphic reactions is disputed (Moulas et al., 2019; Wheeler, 2018).

For the Monte Rosa nappe, specifically within the western portions of the nappe at the head of the Ayas valley, Italy (Figure 2a), recent work by Luisier et al. (2019) reported peak Alpine pressure variations (0.8 ± 0.3 GPa) between a whiteschist (~ 2.2 GPa) and the host metagranite (~ 1.4 GPa; Figure 2b). Based on field and microstructural observations, as well as geochemical analyses, Luisier et al. (2019) proposed that the pressure variations cannot be explained by tectonic mixing (*mélange*), as the whiteschist and metagranite are structurally coherent (documented by cross-cutting post-Variscan dikes). They also excluded complete retrogression of the jadeite-free metagranite and sluggish kinetics due to low water activity. Luisier et al. (2019) suggests that these peak pressure variations could represent tectonic pressure variations.

Here, we test whether the whiteschist HP imprint of 2.2–2.5 GPa represents regional, ‘whole-nappe’, metamorphic conditions or local deviations, within the upper Ayas valley region (Figure 2a). We have investigated numerous metapelitic samples from the Monte Rosa basement metasediments, and identified three independent mineral assemblages that are from outcrops structurally continuous with the localities of previous studies (Chopin & Monié, 1984; Luisier et al., 2019; Marger et al., 2019; Pawlig & Baumgartner, 2001). The samples are unique mineral assemblages representing peak Alpine conditions within pseudomorphs of former contact metamorphic minerals, suitable therefore, to understand further the nature and existence of peak pressure variations. The main assemblages we have investigated are stauroilite–chloritoid bearing that are, to the best of our knowledge, the first described occurrences in the Monte Rosa nappe. Stauroilite-bearing assemblages can pose difficulties in thermodynamic modelling, due to the apparent compositional variability (e.g.

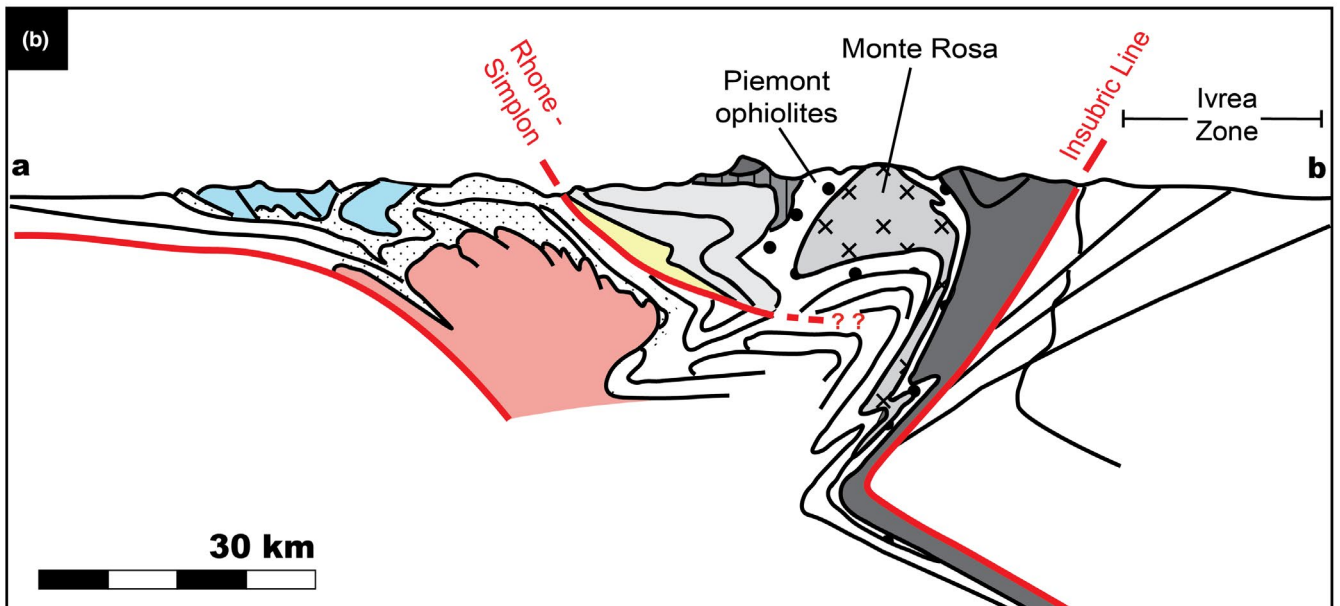
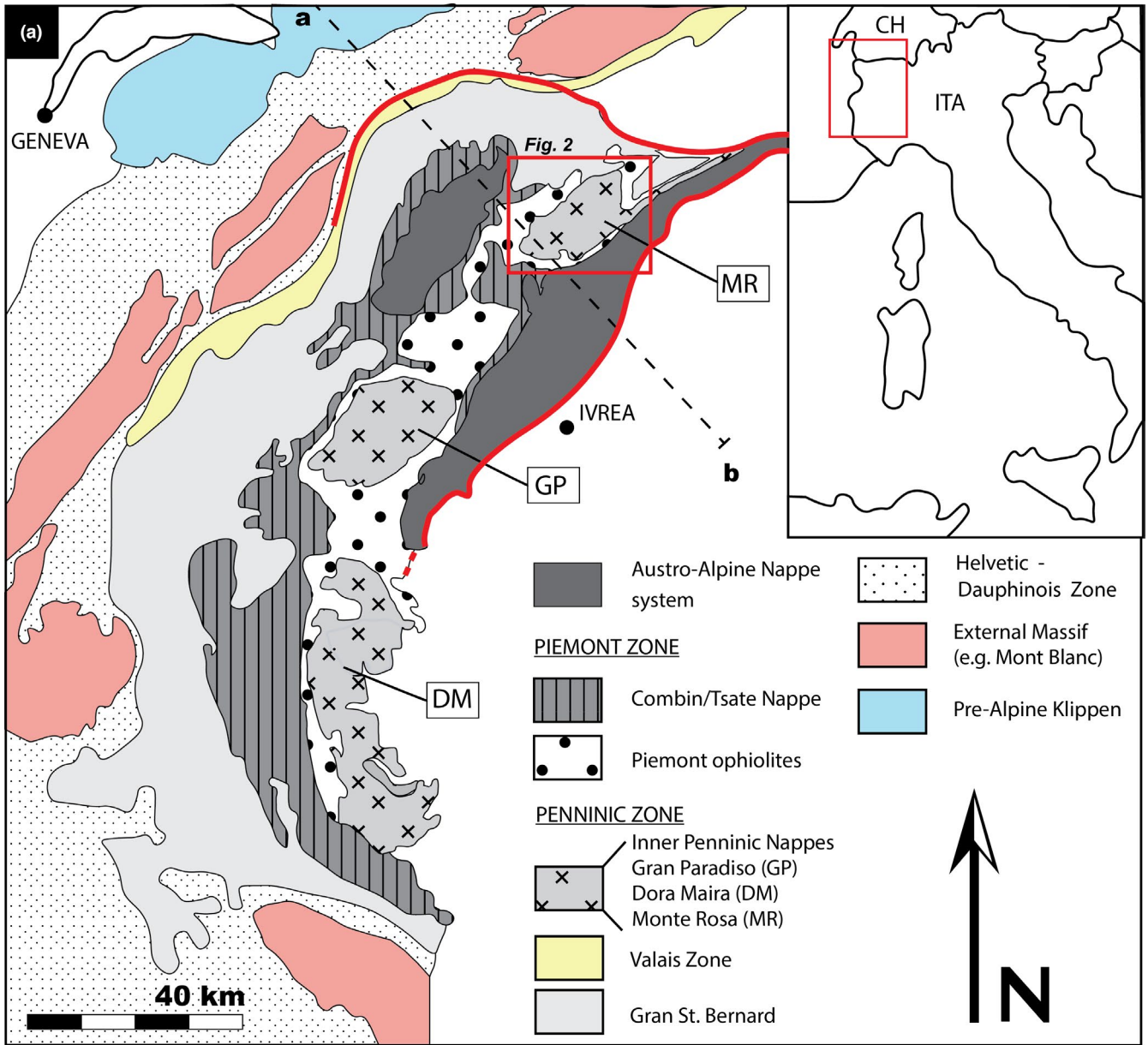


FIGURE 1 (a) Simplified tectonic map of the western Alps showing the major tectonic units; adapted from Beltrando et al. (2010). The Monte Rosa area is in the red box. (b) Simplified cross-section through the western Alps highlighting the Penninic + Piemonte units and major structural discontinuities; modified from figure 23 of Steck et al. (2015). For better visibility and to provide a first-order geometry, we have combined several tectonic units, for example, the pre-Alpine Klippen include the Niesen nappe or the Helvetic–Dauphinois zone includes the Ultrahelvetics. For a detailed tectonic map and section the reader is referred to Steck et al. (2015)

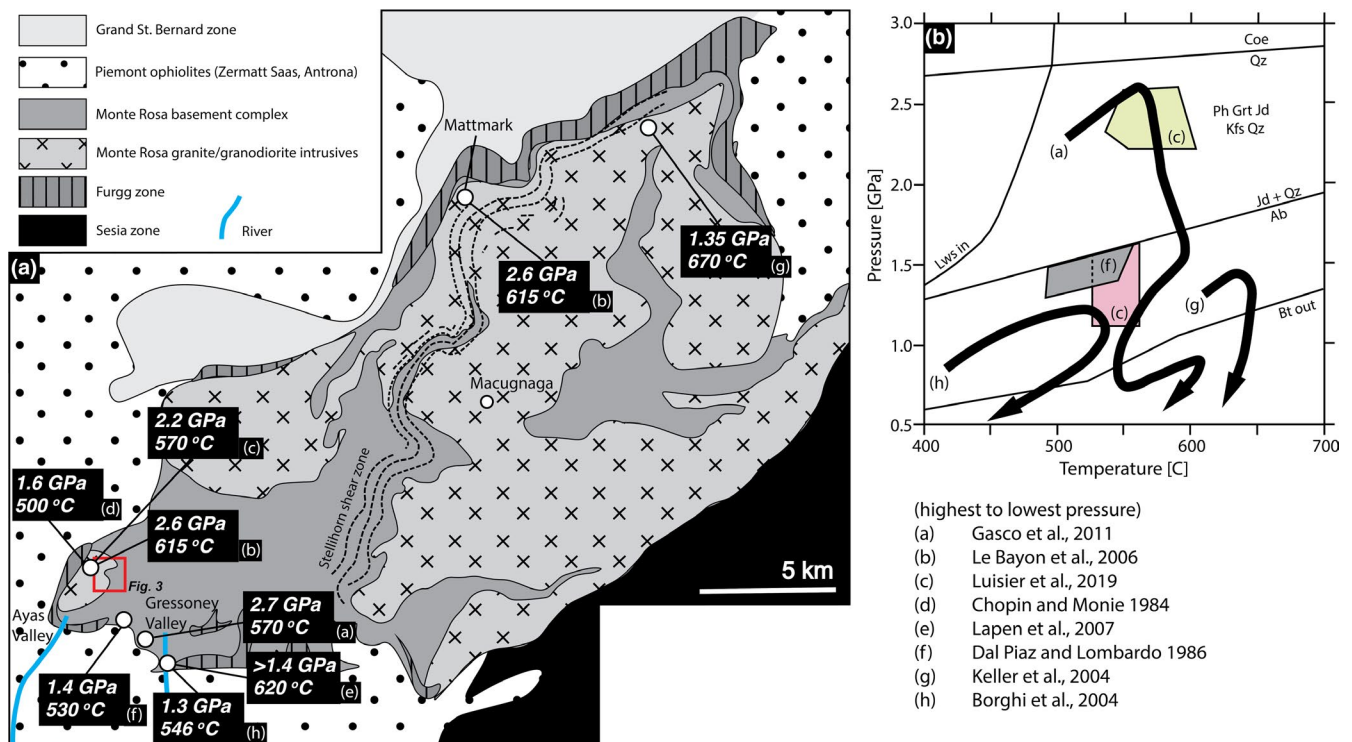


FIGURE 2 (a) Simplified geological map of the Monte Rosa nappe modified after Steck et al. (2015) with estimates of peak Alpine metamorphism from multiple studies (represented from high to low pressure); study area in red box. (b) Pressure–temperature plot of Alpine metamorphism, outlining the peak Alpine pressure disparities, modified after Luisier et al. (2019)

Hawthorne et al., 1993). This variability is primarily the result of unknown site occupations involving Al, Mg, Fe²⁺, Fe³⁺, Ti, Cr, Zn, Co, and Li, as well as H content (Dutrow et al., 1986; Griffen, 1981; Hawthorne et al., 1993; Holdaway et al., 1986; Tuisku et al., 1987). These variabilities, combined with the lack of thermodynamic data for staurolite, require consideration when calculating metamorphic conditions of formation, specifically when applying the appropriate mixing model (e.g. Berman, 1990; Powell & Holland, 1993). For the analysed rocks, we investigate different mixing models and the subsequent effects on pseudosection derived peak pressure and temperature.

2 | GEOLOGICAL SETTING

2.1 | General overview

The Monte Rosa massif, christened the ‘Queen of the Alps’ (King, 1858), is one of the geologically most studied tectonic

units in the Alpine orogenic chain (Dal Piaz, 2001). It belongs to the internal crystalline massifs of the Western and Central Alps, along with the Dora Maira and Gran Paradiso massifs (Figure 1a). These massifs represent dismembered continental crust incorporated into the Eocene-aged Alpine orogeny (Steck et al., 2015). The Monte Rosa massif consists of a pre-Variscan basement, which was intruded by Permian-age granitic bodies (Figure 2a). The current position of the basement complex resides within the collisional Austroalpine–Penninic wedge and lies structurally between the overlying Zermatt–Saas and underlying Antrona ophiolitic sequences (Figure 1b).

The palaeogeographic location of the Monte Rosa unit has been attributed in many earlier studies to the southern Briançonnais domain as part of the European margin (Dal Piaz, 2001; Steck et al., 2015). This domain was separated from the European margin by the Valais basin to the north and bordered by the Piemont basin to the south prior to their subsequent collision during Alpine orogeny.

The Monte Rosa massif consists of lithologies that record a multiphase metamorphic history. This massif was

described as a complex poly-metamorphic basement by Bearth (1952), consisting of high-grade deformed paragneisses and a younger granitic complex, consisting of granitic to granodioritic intrusions and associated dykes. The pre-granitic polymetamorphic basement complex contains metapelites locally preserving a high-grade relict assemblage composed of garnet, biotite, sillimanite, quartz, K-feldspar, cordierite, muscovite and plagioclase (Bearth, 1952; Dal Piaz & Lombardo, 1986). Subsequent petrological investigations of these assemblages revealed a high-*T*, pre-Alpine assemblage related to an upper amphibolite facies sillimanite–K-feldspar metamorphism, $\sim 700^{\circ}\text{C}/0.3\text{--}0.6\text{ GPa}$ (Ferrando et al., 2002), associated with Variscan metamorphism and dated at c. 330 Ma (e.g. Engi et al., 2001). This basement complex was folded and deformed prior to the post-Variscan granitic intrusions dated at $269 \pm 4\text{ Ma}$ (Pawlig, 2001). A contact aureole in the metasediments of the basement complex resulted from the thermal perturbation related to the granitic intrusions, leading locally to partial melting (Dal Piaz, 2001; S1 supplementary material, herein referred to as SM-S(*n*)). Hydrothermal alteration locally overprinting the granite has been documented (Luisier et al., 2019; Marger et al., 2019; Pawlig & Baumgartner, 2001). The Alpine HP eclogite facies metamorphism ($1.2\text{--}2.7\text{ GPa}/490\text{--}640^{\circ}\text{C}$; Borghi et al., 1996; Chopin & Monié, 1984; Ferrando et al., 2002; Gasco et al., 2011; Dal Piaz & Lombardo, 1986; Keller et al., 2004; Lapen et al., 2007; Le Bayon et al., 2006) has been dated at $42.6 \pm 0.6\text{ Ma}$ (Lapen et al., 2007) and retrogression to greenschist facies was dated between 40 and 37 Ma for both the Monte Rosa (Chopin & Monié, 1984) and the overlying Zermatt–Saas units (Skora et al., 2015). Lastly, the Monte Rosa nappe exhibits an albite–oligoclase metamorphic isograd first described by Bearth (1958). This Barrovian-style isograd is similar to other units of the Central Alps (e.g. Lepontine Dome), and suggests a post-peak Alpine regional thermal metamorphic event (Niggli, 1960). Fission track zircon ages indicate that the western region of the Monte Rosa nappe cooled below $\sim 225^{\circ}\text{C}$ at c. 33 Ma (Hurford et al., 1991). Hence, the massif was exhumed to a depth less than $\sim 10\text{ km}$ already at c. 33 Ma, assuming a geothermal gradient of $22.5^{\circ}\text{C}/\text{km}$.

2.2 | Previous estimates of peak Alpine PT

We review shortly previous estimates for peak Alpine conditions incurred by basement lithologies of the Monte Rosa nappe, focusing on its western portions, namely the upper Ayas and Gressoney valleys in the southwest portions of the nappe and the Mattmark and Loranco localities (Figure 2a). The western portion of the Monte Rosa nappe is separated from the eastern portion by a structural discontinuity, termed the Stellihorn shear zone (Figure 2a; Steck et al., 2015).

Dal Piaz and Lombardo (1986) described micaschist and metabasalt samples from the upper Gressoney valley (Figure 2a). Micaschist peak HP paragenesis consists of Ph, Cld, Grt, Ky \pm Gln (mineral abbreviations after Whitney & Evans, 2010). Metabasaltic peak paragenesis consists of Grt, Omp, Gln, Rt, Pg \pm Qz \pm Zo. Peak pressure was constrained at 1.4 GPa due to the absence of jadeite within the metagranite via the reaction $\text{Ab} = \text{Jd} + \text{Qz}$ (Dal Piaz & Lombardo, 1986; Holland, 1979). The minimum pressure was estimated at 0.8–1.0 GPa, using jadeite and omphacite molar contents of pyroxene within metabasalt samples (Holland, 1979). Minimum temperature estimates were defined by the paragonite-in reaction in metabasalts: $\text{Lws} + \text{Ab} = \text{Pg} + \text{Qz} + \text{H}_2\text{O}$ (Holland, 1979). Maximum temperature is constrained via the chloritoid-out reaction in micaschists: $\text{Cld} + \text{Qz} = \text{St} + \text{Grt} + \text{H}_2\text{O}$ (Rao & Johannes, 1979). Peak temperature ranges were refined using the garnet–clinopyroxene thermometer from Ellis and Green (1979) between 440 and 530°C .

Borghi et al. (1996) sampled metapelitic and metabasic lithologies from the upper Gressoney valley. High-*P* minerals consist of Qtz, Ab, Ph, Pg, Chl, Grt, Ky, Cld, Gln, Rt, and Ep. Peak pressure from silica content of phengite (Massonne & Schreyer, 1987) and peak temperature from garnet–phengite reveal a minimum pressure of 1.3 GPa and a temperature of $546 \pm 21^{\circ}\text{C}$.

Keller et al. (2004) examined two metapelitic samples from a continuous structural layer involved within a shear zone from the Loranco locality (Figure 2). The shear zone is interpreted to represent peak Alpine HP conditions, partially preserving pre-Alpine mineral assemblages. The HP paragenesis consists of Ph, Pg, Qz, Grt, Pl, Ky, Ilm, Rt, and Tur. The resulting stability field is between $620\text{--}670^{\circ}\text{C}$ and 1.20–1.35 GPa, via thermodynamic modelling using Berman (1988), update 92 database, constrained also by the lack of granite anatexis (Huang & Wyllie, 1974).

Gasco et al. (2011) investigated metapelitic samples and metabasic samples from a mafic boudin within the Monte Rosa basement micaschists in the upper Gressoney valley, close to the tectonic contact with the structurally higher Zermatt–Saas unit (Figure 2). Eclogite metabasic boudins represent a mineral assemblage of Omp, Gln, Grt, Ph, Lws, Rt, and Qz, presumably equilibrated at peak conditions at 2.4–2.7 GPa and $550\text{--}570^{\circ}\text{C}$ (Holland & Powell, 1998, update 2004). Metapelite assemblages of Ph, Pg, Grt, Chl, Ab/ Olig, Hbl, Qz, Rt, Ilm \pm Bt, are interpreted to represent re-equilibration during decompression at 0.7–0.9 GPa and $550\text{--}600^{\circ}\text{C}$.

Peak Alpine HP conditions have also been calculated from assemblages within the Monte Rosa metagranites known as ‘whiteschists’, consisting of chloritoid, talc, phengite, and quartz \pm garnet or kyanite (Chopin & Monié, 1984; Le Bayon et al., 2006; Marger et al., 2019). A refinement of these

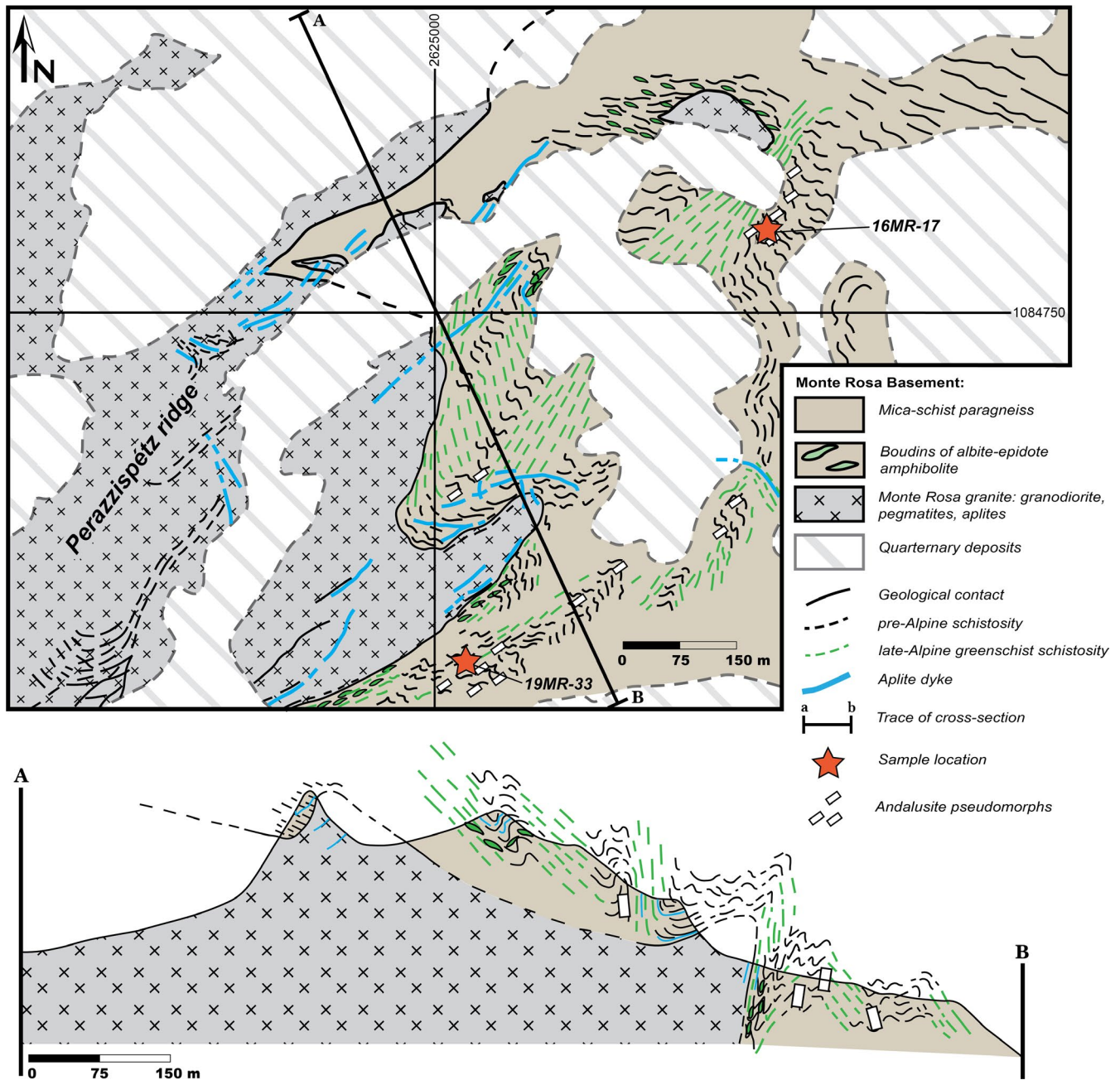


FIGURE 3 Geological map and cross-section of the ‘Peraz’ study area in the western Monte Rosa basement and metagranite, including the location of metapelite samples taken for this study (Red stars). Note the separation of pre-Alpine and late-Alpine schistosity

estimates has recently been made by Luisier et al. (2019; Figure 2b). This unique assemblage has a protolith chemistry deriving from the late magmatic metasomatic alteration of the host granite (Pawlig & Baumgartner, 2001). The peak pressure paragenesis indicates approximately 2.2 ± 0.2 GPa at 540–600°C (Luisier et al., 2019). Peak Alpine conditions were also estimated for the host/protolith metagranite. Peak metamorphic assemblages consist of phengite + titanite pseudomorphs replacing biotite, as well as fine-grained pseudomorphs after plagioclase, consisting of albite + zoisite \pm phengite \pm garnet. These parageneses, as well as additional

pressure estimates based on Si content in phengite, combined with water activity estimates, and the lack of jadeite within the metagranite, prompted the interpretation that the metagranite never experienced pressures over 1.6 GPa (at temperature 540–600°C).

2.3 | Study area

We have investigated metapelitic samples in the western extent of the Monte Rosa basement in a region termed the

'Cirque du V éraz' (personal communication with G. Dal Piazz) within the upper Ayas valley, Italy (Figures 2 and 3). Due to recent glacial retreat, a newly exposed area has become accessible for detailed geological mapping and sampling (Figure 3). The field area provides an exposed section through the Monte Rosa basement complex up to the overlying Zermatt–Saas Unit. Geometrically, the study area has a domal structure with Monte Rosa metagranites residing within the core of the dome, overlain sequentially by Monte Rosa polymetamorphic basement metapelites, locally overlain by a thin layer of Furgg zone metasediments, and eventually the tectonic contact with the overlying Zermatt–Saas units. The locality is situated directly on the antiformal trace of the backfold, which pervasively affects the nappe (Steck et al., 2015; Figures 1a and 3). High strain domains typically display late-Alpine metamorphism and deformation, equilibrated to greenschist facies during decompression (Figures 3 and 4c). The basement complex locally preserves pre-Alpine structures in low strain domains (Figure 3), whose mineral

assemblages were re-equilibrated during peak Alpine metamorphism (Figure 4c,d).

Samples were obtained east of the Perazzisp étz ridge (Swiss coordinates E: 2626459 N: 84117 alt: 3,302 m and E: 2626048 N: 83526 alt: 2,920 m, Figures 3 and 4). The samples consist of layered metapelites (Figure 4b,c) recording a pre-Alpine foliation. Locally, granitic dikes crosscut the foliation (Figure 4b), attesting to the pre-Alpine age of the main deformation seen in these outcrops. We report few samples of former aluminosilicate-bearing contact metamorphic metapelites that were subsequently equilibrated at HP conditions (Figure 4d and Figure SM-S2). The peak Alpine metamorphic minerals are observed within pseudomorphs replacing former larger pre-Alpine minerals (Figure 4d and Figure SM-S3). The presence of pre-Alpine dykes crosscutting metapelite lithologies (Figure 4a,b), and migmatite textures associated with pre-Alpine granitic intrusion (Figure SM-S1) indicate that this area represents a structurally coherent tectonic body, and not a tectonic mélangé.

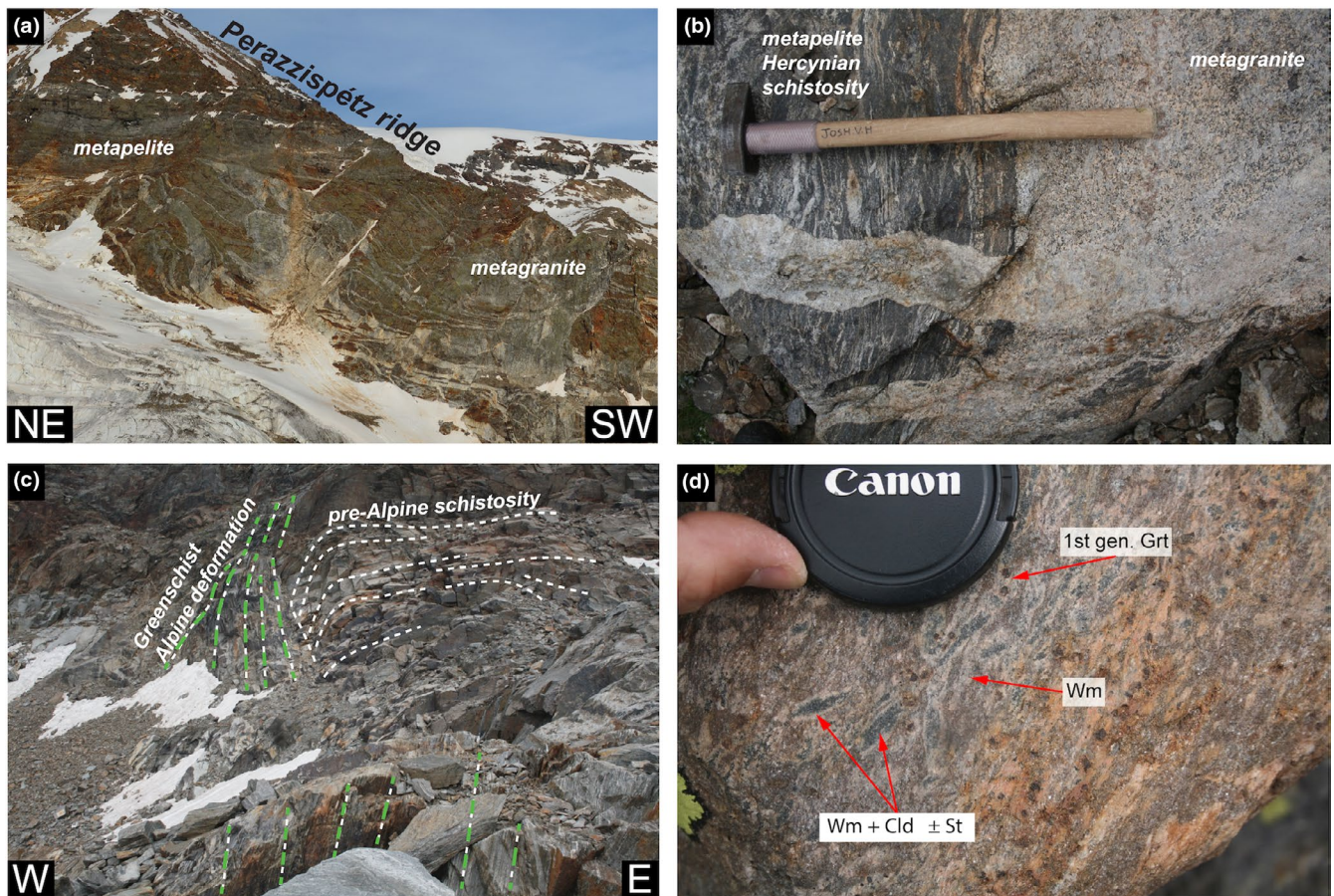


FIGURE 4 Representative field images for the study area and metapelitic samples: (a) outcrop of basement metapelites intruded by metagranites (note aplitic dykes), (b) aplitic dyke of the Permian Monte Rosa metagranite cross-cutting gneisses of the Monte Rosa basement, (c) deformed metapelitic basement showing horizontal pre-Alpine deformation sheared and deformed by vertical late Alpine greenschist facies shear zones, (d) domains of preserved peak Alpine assemblages (mineral abbreviations after Whitney and Evans (2010))

3 | METHODOLOGY

3.1 | Analytical methods

Electron probe microanalysis (EPMA) of major and minor element compositions of white mica, chloritoid, staurolite, garnet, and chlorite were conducted using a JEOL JXA-8350F HyperProbe at the University of Lausanne, Switzerland. In total, quantitative analysis of 46 white mica grains (197 points), 11 chloritoid grains (149 points), 12 staurolite grains (68 points), 8 garnet grains (72 points), and 5 chlorite grains (30 points) was undertaken. The operating conditions were 15.0 kV acceleration voltage and $1.5\text{--}2.0 \times 10^{-8}$ A, with a beam diameter of 5.0 μm . Natural minerals were used as reference materials: orthoclase (K_2O , SiO_2), andalusite (Al_2O_3), albite (Na_2O), fayalite (FeO), forsterite (MgO), tephrite (MnO), wollastonite (CaO), sphalerite (ZnO), and rutile (TiO_2). Structural formulae from Howie et al. (1992) were used for stoichiometric calculations on the basis of 11 oxygen for white mica, 8 cations for chloritoid, 12 oxygen for garnet, and 13 oxygen for chlorite ($(\text{Mg}, \text{Fe})_5\text{Al}[\text{AlSi}_3\text{O}_{10}](\text{OH})_8$). For staurolite ($(\text{Fe}^{+2}, \text{Mg}, \text{Zn})_{3-4}(\text{Al}, \text{Fe}^{+3}, \text{Ti})_{17-18}\text{O}_{16}[(\text{Si}, \text{Al})\text{O}_4]_8\text{H}_{3-4}$ (Deer et al., 2013)), normalization assuming $\text{Si} + \text{Al} - \frac{1}{3}\text{Li} + \frac{2}{3}\text{Ti} + \text{Fe}^{3+} = 25.55$ cations as proposed in Holdaway et al. (1991) was used, due to uncertainties in H and Fe^{3+} content.

3.2 | Thermodynamic modelling

Phase diagrams were calculated using the THERIAK-DOMINO software suite (de Capitani & Brown, 1987) in combination with the Berman database (Berman, 1988, 92 update). This database was chosen in order to: (a) have an internally consistent database, and (b) to accurately compare thermodynamically calculated pressure and temperature with results of the study of Luisier et al. (2019). Bulk compositions were calculated based on quantitative image analysis of equilibrium subdomains in each sample, using EPMA-derived mineral compositions, along with the MATLAB© based image processing software XMapTools (Lanari et al., 2014), in the chemical system NCKFMASH (Figures SM-S7 and S11). Solution models used are after the 92 update of Berman (1988) which include: H_2O after the HAAR equation of state (Kell et al., 1984), white mica after Massonne and Szpurka (1997), chloritoid, garnet and chlorite after the 92 update of Berman (1988), and staurolite after Nagel et al. (2002).

The current solution model data for staurolite consider only Fe and Mg end-members (Nagel et al., 2002). However, a wealth of literature highlights a wider range of possible staurolite end-members (e.g. Zn; e.g. Holdaway et al., 1991). In order to account for the lack of variability in experimentally derived end-member thermodynamic data, for example,

Zn in staurolite, we have employed a method to adjust the activity of available solid solution end-member data (Nagel et al., 2002). To do so, the activity ($\alpha_i^{\text{reduced}}$) for Mg and Fe staurolite end-members were reduced to account for the Zn end-member (see Appendix 1). The thermodynamic data of the end-member staurolites were adjusted, using two mixing models to account for the Zn concentrations analysed, within the JUN92B database by Berman (1988) utilized by THERIAK-DOMINO. Both models assume ideal mixing: model 1 assumes molecular mixing, while model 2 assumes site mixing. We adjust the thermodynamic properties of Fe and Mg staurolite end-members using an entropy correction, $S_{\text{eff}}^{T_0, P_0} = S_{\text{MgSt}}^{T_0, P_0} - R \ln(\alpha_i^{\text{reduced}})$ (see Appendix 1 for full derivation). PT errors are estimated from the resulting stability fields calculated with and without the entropy correction for staurolite-bearing assemblages.

4 | PETROGRAPHIC DESCRIPTIONS

In order to capture peak Alpine conditions, samples were taken from within the Monte Rosa polymetamorphic basement that has experienced little to no late Alpine metamorphic and deformational overprint (Figures 3 and 4c). The two samples analysed (16MR-17 and 19MR-33) were taken from close proximity to each other (Figure 3). These samples are metapelites, which show different mineral paragenesis due to variable protolith chemistry.

4.1 | Sample 16MR-17

Sample 16MR-17 displays a weakly inherited foliation defined by an assemblage of fine-grained quartz + white mica + garnet + chlorite, wrapping around large garnet porphyroblasts, as well as domains consisting of a fine-grained assemblage of staurolite, chloritoid, phengite, and paragonite (Figure 5a–c and Figure SM-S4). These fine-grained domains have a pseudomorph texture, presumably after a larger mineral, due to their sharp boundaries and regular form (Figure 5a and Figure SM-S4). Accessory minerals are apatite, rutile, tourmaline, ilmenite, zircon, and monazite. Late matrix phases consist of biotite, replacing garnet, and chlorite, partially replacing garnet and biotite (Figure 5e). Two generations of garnet exist (Figure 5b). Larger garnet porphyroblasts represent an older first-generation Grt. A second generation of smaller garnet (second-generation Grt) are embedded in a fine-grained matrix of white mica (phengite + paragonite, Figure 5b) and minor amounts of quartz and chlorite (Figure 5e). First-generation garnet show dark dissolution–precipitation rims marked by fine inclusions of an unknown mineral (Figure 5b). These dark precipitation

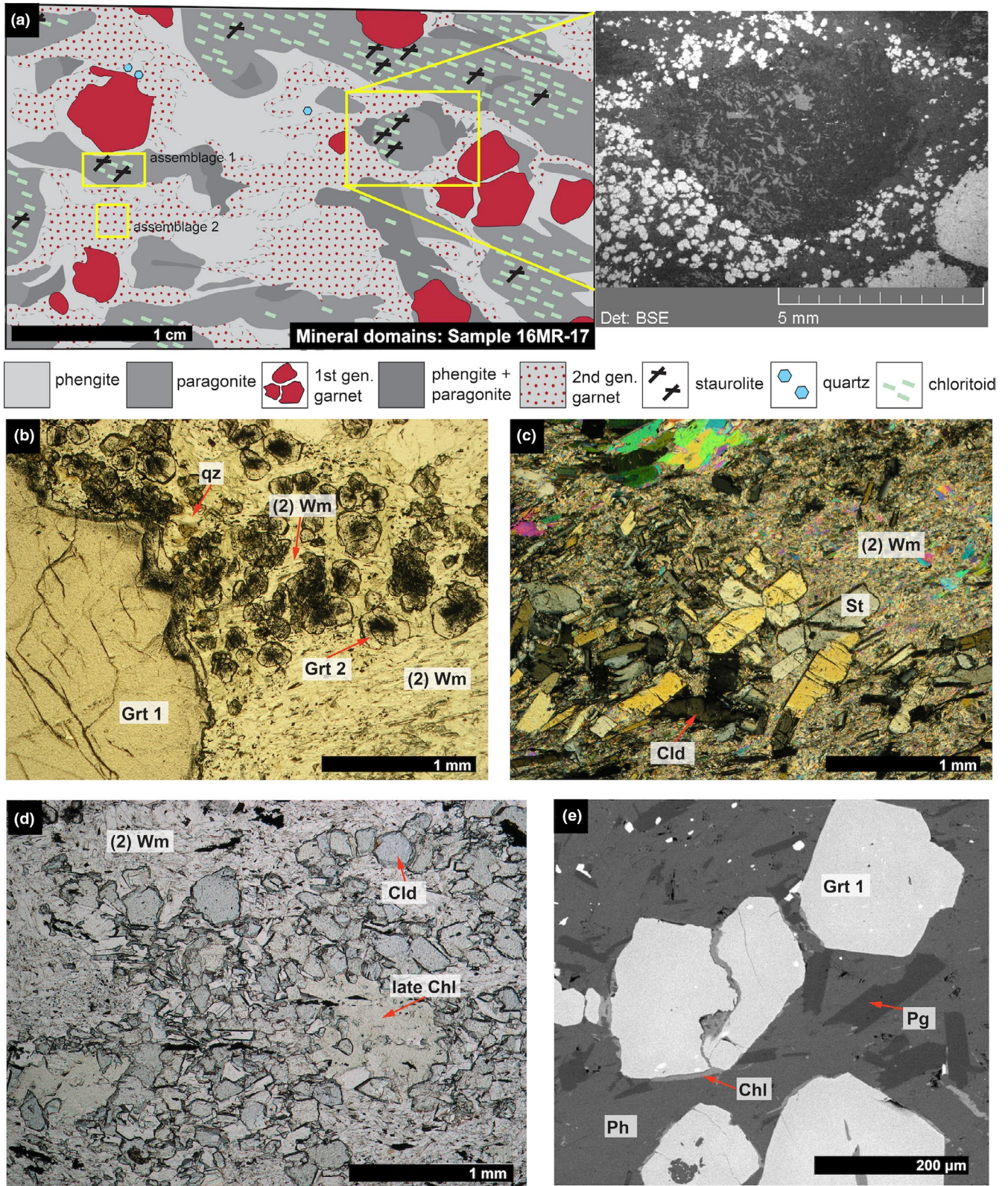


FIGURE 5 Representative petrological images for the study area and metapelitic samples: (a) textural and compositional domains for sample 16MR-17 including SEM image of typical assemblage 1 and 3 pseudomorph form, (b) plane polarized light image of sample 16MR17 showing the two generations of garnet (assemblage 2), (c) cross-polarized light image of sample 16MR17 showing staurolite-chloritoid-bearing assemblage (assemblage 1), (d) plain-polarized image of sample 19MR-33 showing chloritoid, white mica and late chlorite (assemblage 3), and (e) SEM image of typical assemblage 2 textures. Mineral abbreviations after (Whitney & Evans, 2010)

TABLE 1 Representative microprobe analysis (16MR-17 and 19MR-33)

Analysis	Assemblage 1					Assemblage 2					Assemblage 3				
	Phengite	Paragonite	Chloritoid	Staurolite	Phengite	Phengite	Paragonite	Rim	Paragonite	Garnet	Chlorite	Phengite	Paragonite	Chloritoid	
	Core	Rim	Core	Rim	Core	Core	Core	Core	Core	Core	Core	Core	Core	Core	
SiO ₂	48.65	47.11	24.96	28.19	50.05	48.02	46.28	37.11	46.28	37.51	25.86	47.52	47.59	24.12	
Al ₂ O ₃	32.44	40.01	42.10	52.91	28.50	31.84	40.01	20.86	40.01	20.83	21.59	34.63	40.85	42.69	
TiO ₂	0.25	0.08	0.11	0.33	0.18	0.25	0.05	0.02	0.05	0.41	0.08	0.57	0.04	0.01	
MnO	0.03	0.00	0.00	0.03	0.00	0.00	0.01	0.59	0.01	1.50	0.05	0.01	0.00	0.10	
ZnO	0.03	0.00	0.00	4.74	0.00	0.02	0.00	0.02	0.00	0.00	0.11	0.02	0.00	0.08	
FeO	1.35	0.26	20.40	9.59	1.70	1.27	0.33	36.49	0.33	30.54	20.10	1.59	0.61	22.94	
MgO	2.05	0.10	5.32	1.81	3.21	2.18	0.08	3.50	0.08	2.72	18.27	1.20	0.08	3.90	
Na ₂ O	0.96	7.14	0.01	0.09	0.48	0.86	7.07	0.011	7.07	0.00	0.01	1.32	7.08	0.00	
CaO	0.00	0.13	0.00	0.01	0.00	0.00	0.42	1.41	0.42	6.74	0.01	0.02	0.06	0.01	
K ₂ O	9.70	1.11	0.10	0.01	10.43	10.08	0.69	0.01	0.69	0.01	0.06	9.58	0.70	0.01	
F	0.25	0.04	—	—	—	—	—	—	—	—	—	—	—	—	
Cl	0.01	0.00	—	—	—	—	—	—	—	—	—	—	—	—	
Total	95.71	95.97	93.00	97.71	94.55	94.52	94.56	100.04	94.56	100.29	86.13	96.45	97.01	93.86	
Normalized ^a	11 (a)	11 (a)	8 (a)	25.55 (c) ^b	11 (a)	11 (a)	11 (a)	12 (a)	11 (a)	12 (a)	13 (a)	11 (a)	11 (a)	8 (a)	
Si ⁴⁺	3.22	2.99	2.00	7.95	3.36	3.21	2.98	2.99	2.98	2.99	2.51	3.12	2.98	1.94	
Al ³⁺	2.53	2.99	3.98	17.58	2.25	2.51	3.03	1.96	3.03	1.96	2.47	2.68	3.02	4.04	
Ti ⁴⁺	0.01	0.00	0.00	0.07	0.01	0.02	0.00	0.00	0.00	0.03	0.01	0.03	0.00	0.00	
Mn ²⁺	0.00	0.00	0.01	0.01	0.00	0.00	0.00	0.04	0.00	0.10	0.00	0.00	0.00	0.01	
Zn ²⁺	0.00	0.00	0.01	0.99	0.00	0.00	0.00	0.00	0.00	0.00	0.01	0.00	0.00	0.01	
Fe ²⁺	0.08	0.01	1.37	2.26	0.10	0.08	0.02	2.46	0.02	2.04	1.63	0.09	0.03	1.54	
Mg ²⁺	0.20	0.01	0.64	0.76	0.32	0.23	0.01	0.42	0.01	0.32	2.64	0.12	0.01	0.47	
Na ⁺	0.12	0.88	0.00	0.00	0.06	0.11	0.88	0.00	0.88	0.01	0.00	0.17	0.86	0.00	
Ca ²⁺	0.00	0.01	0.00	0.00	0.00	0.00	0.00	0.12	0.00	0.58	0.00	0.00	0.00	0.00	
K ⁺	0.82	0.09	0.00	0.00	0.89	0.86	0.06	0.00	0.06	0.00	0.01	0.80	0.06	0.00	
F	0.00	0.00	—	—	—	—	—	—	—	—	—	—	—	—	
Cl	0.00	0.00	—	—	—	—	—	—	—	—	—	—	—	—	
Total	6.98	6.98	8.01	29.62	6.99	7.02	6.98	8.01	6.98	8.01	9.28	7.01	6.96	8.01	

^aNormalization using anions (a) and cations (c).^bNormalization after Holdaway et al. (1991).

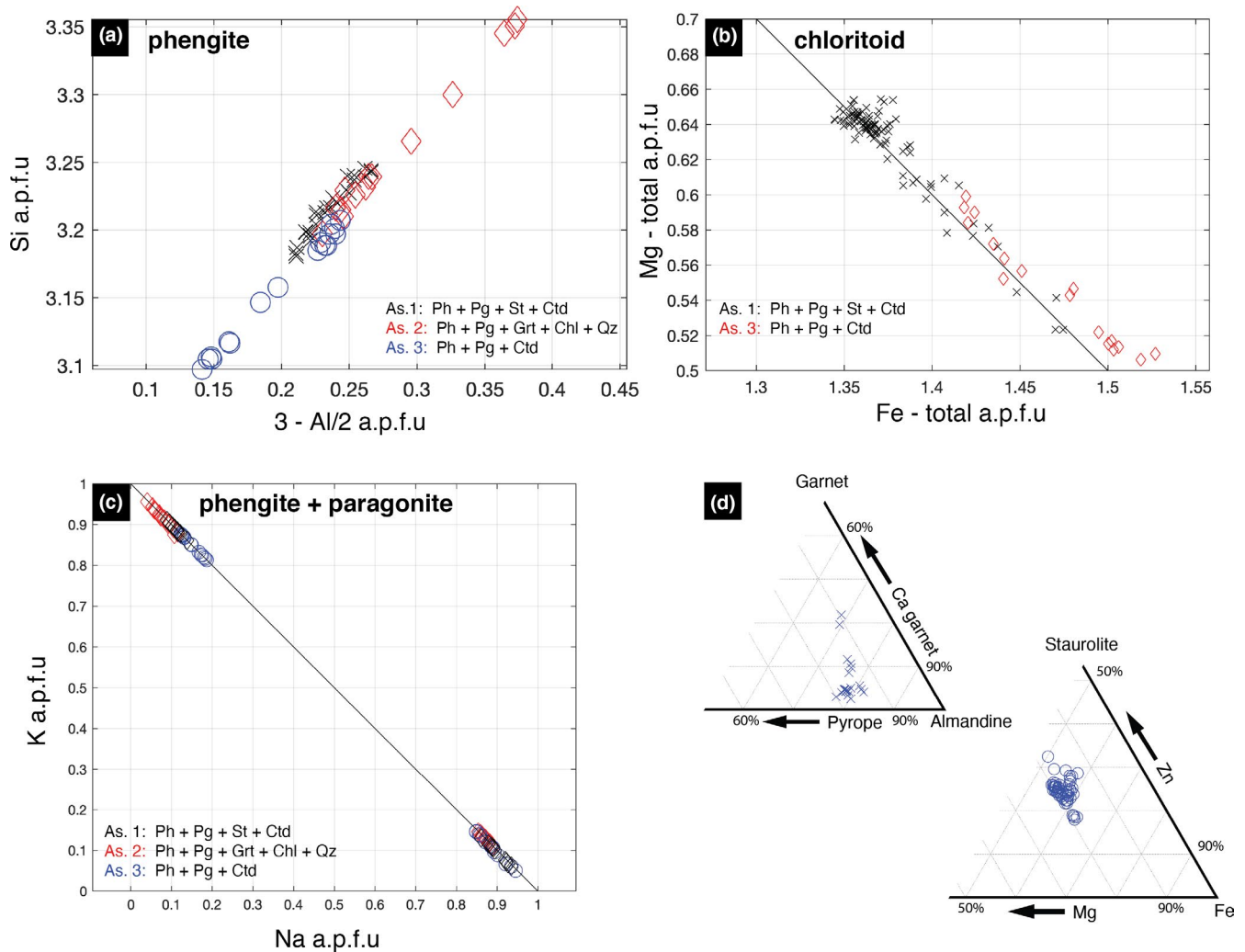


FIGURE 6 Normalized mineral chemical data for assemblages 1, 2, and 3 (sample 16MR-17 and 19MR-33): (a) Si in phengites against Al tetrahedral site, (b) chloritoid Mg and Fe-total, (c) Na in paragonite and K in phengite mixing gap of white mica, and (d) ternary plot for garnet compositions in assemblage 2, and ternary plot for staurolite compositions in assemblage 1 (note non-negligible Zn)

growth rims coincide with the smaller second-generation garnet, which have inclusion rich cores (Figure 5b). The schistosity defined by white mica envelops first-generation garnet suggesting the garnet grew pre- or syn-tectonically (Figure 5b). However, second-generation garnet grow statically and post-tectonically with undeformed white mica (Figure 5e). Second-generation garnet is observed to grow statically over former pressure shadows associated with first-generation garnet (Figure 5b).

Based on textural domains, two equilibrium assemblages were defined that are interpreted to have captured peak Alpine metamorphic conditions. Assemblage 1 consists of domains of staurolite, chloritoid, phengite, and paragonite, pseudomorphing former andalusite, as highlighted in Figure 5a and Figure SM-S3. The whole pseudomorph domains after andalusite have grown statically, with un-oriented mica and staurolite twins (Figure 5c). Assemblage two consists of second-generation garnet, phengite, paragonite, chlorite,

and quartz (Figure 5b,e). Assemblages 1 and 2 are statically grown and therefore post-kinematic.

4.2 | Sample 19MR-33

Sample 19MR-33 is texturally and petrologically similar to 16MR-17. However, no staurolite is observed in the fine-grained pseudomorph domains that characterize assemblage 1, only chloritoid is present in a matrix of phengite and paragonite (Figure 5d).

5 | MINERAL CHEMISTRY

Representative compositional results for phengite, paragonite, chloritoid, and staurolite in assemblage 1, as well as phengite, paragonite, garnet, and chlorite in assemblage 2 of

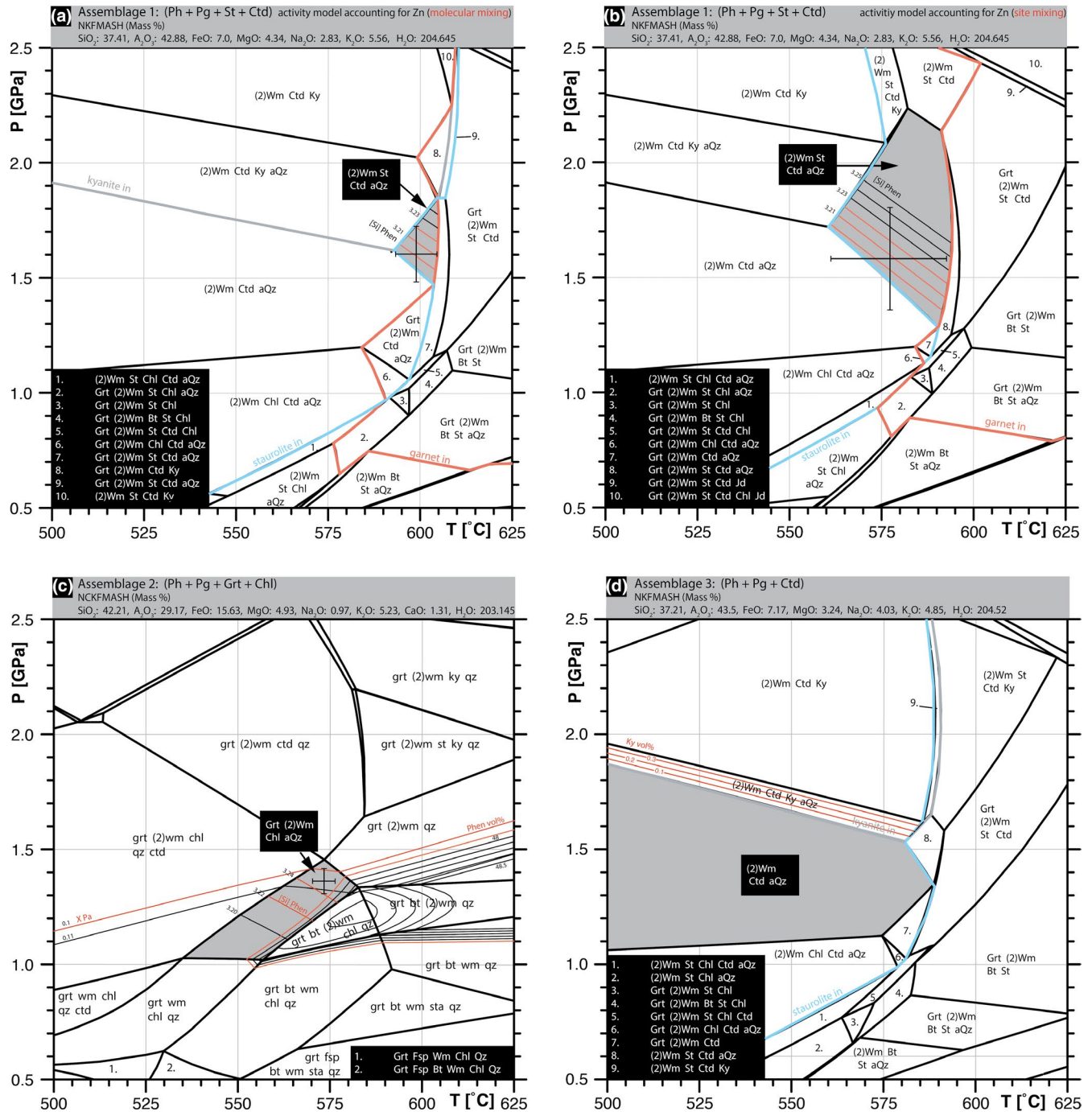


FIGURE 7 Thermodynamic pseudosection modelling for assemblages 1, 2, and 3 (sample 16MR17 and 19MR33) using the Theriak/Domino software and JUN92 Berman database (Berman, 1988): (a) assemblage 1 results in NCKFMASH with reduced activity for Mg–Fe end-member solutions based on molecular mixing assumption (a.p.f.u. isopleths for Si in phengite), (b) assemblage 1 results in NCKFMASH with reduced activity for Mg–Fe end-member solutions based on site mixing assumption (a.p.f.u. isopleths for Si in phengite), (c) assemblage 2 results in NCKFMASH (a.p.f.u. isopleths for Si in phengite, X paragonite and phengite vol%), and (d) assemblage 3 results in NCKFMASH system (a.p.f.u. isopleths for kyanite vol%)

sample 16MR-17 and phengite, paragonite, chloritoid in assemblage 3 of sample 19MR-33 are displayed in Table 1. In assemblage 1, two white mica are distinguished. Phengite has Si content ranging between 3.18 and 3.25 a.p.f.u., which is correlated with an increase in the Tschermak component between 0.18 and 0.25 (Figure 6a). Phengites have a K content

ranging between 0.85 and 0.91 a.p.f.u. (Figure 6c). Phengite coexists with paragonite with a Na content between 0.83 and 0.87 a.p.f.u. (Figure 6c). Chloritoid compositions are relatively richer in Fe compared to Mg, with an X_{Mg} (Mg/(Mg + Fe)) between 0.26 and 0.33. Similarly, staurolite is Fe rich, with a X_{Fe} (Fe/(Mg + Fe)) of 0.68–0.74 (Figure 6b).

The high content of zinc is remarkable in staurolite, reaching 1.0 a.p.f.u. in some samples (Figure 6d; Table 1). No Zn was found by EPMA analysis in any other mineral.

For assemblage 2 of sample 16MR-17, two white mica are also present. Phengite has Si content ranging between 3.20 and 3.37 a.f.p.u., which correlates with an increase in the Tschermak component between 0.20 and 0.37 (Figure 6a). Notably, the highest Si contents are typically within the core of phengite and the lowest at the rim (Table 1). Compared to assemblages 1 and 3, Si content of phengite are highest in this quartz-bearing assemblage. Phengites have a K content ranging between 0.85 and 0.96 a.p.f.u. (Figure 6c). Phengite coexists with paragonite with a Na content between 0.85 and 0.89 a.p.f.u. (Figure 6c). Garnet compositions are almandine rich (Figure 6d) with Fe ranging between 1.41 and 1.55 a.p.f.u. and minimal zoning is observed (Figure SM-S10).

For assemblage 3 of sample 19MR-33, two white mica are also distinguished. Phengite has Si content ranging between 3.10 and 3.21 a.f.p.u., which correlates with an increase in the Tschermak component between 0.10 and 0.21 (Figure 6a). Phengites have a K content ranging between 0.81 and 0.88 a.p.f.u. (Figure 6c). Phengite coexist with paragonite with a Na content between 0.85 and 0.95 a.p.f.u. (Figure 6c). Chloritoid compositions are enriched in Fe (1.41 and 1.55 a.p.f.u.) compared to Mg ranging between 0.50 and 0.59 a.p.f.u. (Figure 6b).

6 | PHASE PETROLOGY

Due to the minimal compositional zoning of all minerals, a pseudosection approach was used in order to calculate PT conditions at fixed bulk-rock composition. Figure 7a,b show the pseudosection results in the NCKFMASH system (SiO_2 - Al_2O_3 - FeO - MgO - K_2O - Na_2O - H_2O) with the bulk compositions displayed for assemblage 1 (phengite + paragonite + staurolite + chloritoid). The stability field of assemblage 1 was well constrained at 1.6 ± 0.05 GPa and $605 \pm 2^\circ\text{C}$. The results for the entropy correction, due to Zn, based on a 'molecular mixing' model are presented along with Si in phengite isopleths (Figure 7a). The new stability field for this assemblage is comparatively larger, expanding towards lower temperatures and higher pressures, resulting in 1.6 ± 0.1 GPa at $600 \pm 5^\circ\text{C}$. The new stability field resulting from the 'site mixing' correction is larger than the 'molecular mixing' model and results in 1.6 ± 0.2 GPa at $585 \pm 15^\circ\text{C}$ (Figure 7b). The appearance of staurolite is shifted towards lower temperatures in comparison with the results using the molecular mixing model in Figure 7a and the classical solution model. Equally, the pseudosection calculations for this assemblage predicts quartz (<1%). However, we have not observed quartz in these staurolite-chloritoid-bearing assemblages.

Representative compositional microprobe results for assemblage 2 from sample 16MR-17 are displayed in Table 1 (garnet + phengite + paragonite + chlorite). Minor zoning is observed in phengite, namely high Si-content in the core of phengites, up to 3.37 a.p.f.u. (Figure 6a). Similarly, minor zoning of Ca and Mn can be observed in garnet (Table 1). Therefore, we took average compositions of Si, Ca, and Mn of phengite and garnet respectively, as input for bulk-rock compositions. Figure 7c shows pseudosection results in the NCKFMASH system (SiO_2 - Al_2O_3 - FeO - MgO - K_2O - Na_2O - CaO - H_2O). Using isopleths for the modal volume of chlorite (vol%), Xparagonite and Si in phengite (a.p.f.u.), the stability field for the observed mineral assemblage ranges from 1.3 to 1.4 GPa at $\sim 575^\circ\text{C}$ (Figure 7c).

Representative composition microprobe results for assemblage 3 from sample 19MR-33 are displayed in Table 1 (phengite + paragonite + chloritoid). We observe minimal zoning in this assemblage with similar values as assemblage 1 (Ph + Pg + St + Ctd). Bulk compositions are similar to assemblage 1 with the exception of lower Zn values. The stability field for the peak paragenesis is large, spanning a wider field of pressures and temperatures (Figure 7d). At temperatures of 575°C , inferred from assemblages 1 and 2, pressure ranges between 1.1 and 1.6 GPa.

7 | DISCUSSION

7.1 | Estimating peak Alpine conditions

Due to the complexity of the polymetamorphic Monte Rosa basement, three periods of geological activity may be responsible for the formation of assemblages 1, 2, and 3, that we interpret to have formed during peak Alpine conditions. These events include (from oldest to youngest): (a) HT-LP Variscan orogenesis, (b) peak high-*P* Alpine orogenesis, and (c) a late Alpine thermal pulse. However, field occurrences, textural relationships and petrological investigations from this study, enable us to attribute the investigated assemblages to equilibration during peak Alpine conditions (Figure 7).

Typically, the studied assemblages occur within centimetre-sized pseudomorphs in low-strain domains (Figures 3 and 4c,d; Figure SM-S3). These pseudomorphs occur close to the late Palaeozoic metagranite intrusion and associated basement migmatites (Figure 4b). We interpret these pseudomorphs to represent relics of former contact metamorphic andalusite that formed during granite emplacement (Figure SM-S3). Therefore, the staurolite + chloritoid-bearing assemblages post-date granite emplacement and thus post-date Variscan orogenesis. Equally, the calculated P-T results for the assemblages analysed in this study do not agree with the older high-*T* and low-*P* metamorphism, characteristics of the Variscan

orogeny. Our results of 1.6 ± 0.2 GPa and $585 \pm 20^\circ\text{C}$ indicate too high pressures and too low temperatures compared with estimates of 0.3–0.6 GPa and 700°C for Variscan metamorphism (Bearth, 1952; Dal Piaz, 2001; Dal Piaz & Lombardo, 1986; Engi et al., 2001).

Another argument for the Alpine formation of the assemblages investigated, is the apparent enrichment of Na (Table 1). This enrichment resulted in the occurrence of large volume proportions of paragonite observed (up to 30%). Similar enrichment in Na of metapelites in close proximity to intrusive bodies has been reported (e.g. Eugster, 1985). These occurrences have been attributed to host-rock interaction with late magmatic hydrothermal fluids. Evidence for post-intrusion hydrothermal activity is also observed in close proximity to our locality, namely the formation of Mg-rich sericite–chlorite schists, that are the precursory equivalent to HP ‘whiteschists’ within the metagranite (Luisier et al., 2019; Marger et al., 2019; Pawlig & Baumgartner, 2001). Associated with hydrothermally induced Mg enrichment of the granite protolith, depletion of Na has been observed (Pawlig & Baumgartner, 2001). The ensuing fluid migration may have contributed to the enrichment of Na in the basement metapelites.

Previous observations of staurolite within the Monte Rosa nappe have been interpreted to be associated with the post-peak Alpine Barrovian metamorphism in the Lepontine dome, far to the East of our finding (Engi et al., 2001; Niggli, 1960, 1970; Niggli & Niggli, 1965). This isograd exists in the far eastern extent below the Monte Rosa nappe pile in the Camugera Moncucco unit (CM), which is structurally one of the deepest unit in the Western Alps (Keller et al., 2004). Observations of relic staurolite have been reported further west from the CM and are linked possibly to a HP Alpine phase, however, no thermodynamic calculations of pressure and temperature have been made (Engi et al., 2001; Niggli, 1970; Niggli & Niggli, 1965). Until now, no observations of staurolite, to the best of our knowledge, in the Monte Rosa nappe have been made west of the Stellihorn shear zone (Figure 2a).

To place the staurolite investigated within the timeframe of the late thermal pulse may pose some difficulties. Firstly, due to the location in the far western portion of the nappe, as Frey et al. (1999) places the western portions of the Monte Rosa nappe at greenschist facies during this time. Secondly, the calculated pressure and temperature within this study have too high pressures at 1.6 ± 0.2 GPa, and even at the lowest structural levels (i.e. within the CM) these pressures would be too high, as Engi et al. (2001) calculated re-equilibration during decompression at conditions of 1.1 ± 0.12 GPa and $652 \pm 41^\circ\text{C}$.

Mineral textures and calculated metamorphic conditions in this study exclude the possibility of equilibration during: (a) Variscan orogenesis, and (3) late Alpine thermal

decompression, therefore, equilibration during (b) peak Alpine conditions remains. The observed assemblages most likely equilibrated in a P – T maximum during Alpine burial. This is observed both texturally and geochemically with garnet growth, as isopleths for garnet growth increase with prograding P – T conditions. Thus, the assemblages investigated here formed during peak Alpine conditions, rather than superimposing them onto a retrogressive pathway during decompression. If these assemblages represent retrogression however, the question remains: from what assemblages did they retrogress? The only pseudomorphic textures we can observe are likely after former andalusite related to Permian-aged contact metamorphism (Figure 4d and Figure SM-S2). However, when comparing calculated P – T equilibrium domains for both assemblages 1 and 2, there does exist a small disparity (Figure 7). Assemblage 1 has ~ 0.2 GPa higher pressures and $\sim 50^\circ\text{C}$ higher temperatures. This is likely due to chlorite replacing garnet (Figure 5e) during retrogression from peak conditions recorded in the staurolite–chloritoid-bearing assemblages along with the influx of H_2O rich fluids. The presented field relations, textural observations, and thermodynamic calculations suggest equilibration during peak Alpine conditions.

7.2 | Sensitivity of thermodynamic mixing models: Zn in staurolite

In order to constrain a reliable Alpine peak pressure and temperature incurred by the Monte Rosa basement, the calculated thermodynamic stability fields must replicate the observed mineral textures, chemistry and modal abundances. Here we will address two caveats in our calculated pseudosections: (i) the presence of Zn in staurolite in assemblage 1, and (ii) the calculated presence of quartz in assemblages 1 and 3.

Concerning caveat (i), we must consider the non-negligible quantities of ZnO measured in staurolite (Table 1). Assessing our microprobe data, staurolite is the only Zn-bearing phase, which is in agreement with other occurrences of Zn-staurolite (e.g. Fox, 1971; Griffen, 1981; Guidotti, 1970; Tuisku et al., 1987). Even with the uniqueness of assemblage 1 of this study (St, Cl, Ms, Pg \pm Qz) as well as the apparent lack of zoning, the range of pressure and temperature varies somewhat considerably when adjusting the existing thermodynamic data of staurolite end-members in the thermodynamic database for Zn (Figure 5a,b). Considering these adjustments, we are able to calculate the new stability fields taken as a whole at 1.6 ± 0.2 GPa and $585 \pm 20^\circ\text{C}$ (Figure 7b). Few authors have investigated the effects of ZnO within staurolite, and similarly reported its large influence on a metamorphic stability field (e.g. Fox, 1971; Holdaway et al., 1991; Tuisku et al., 1987). Considering Zn's large influence on the pressure and temperature range of stability, treating it as an additional

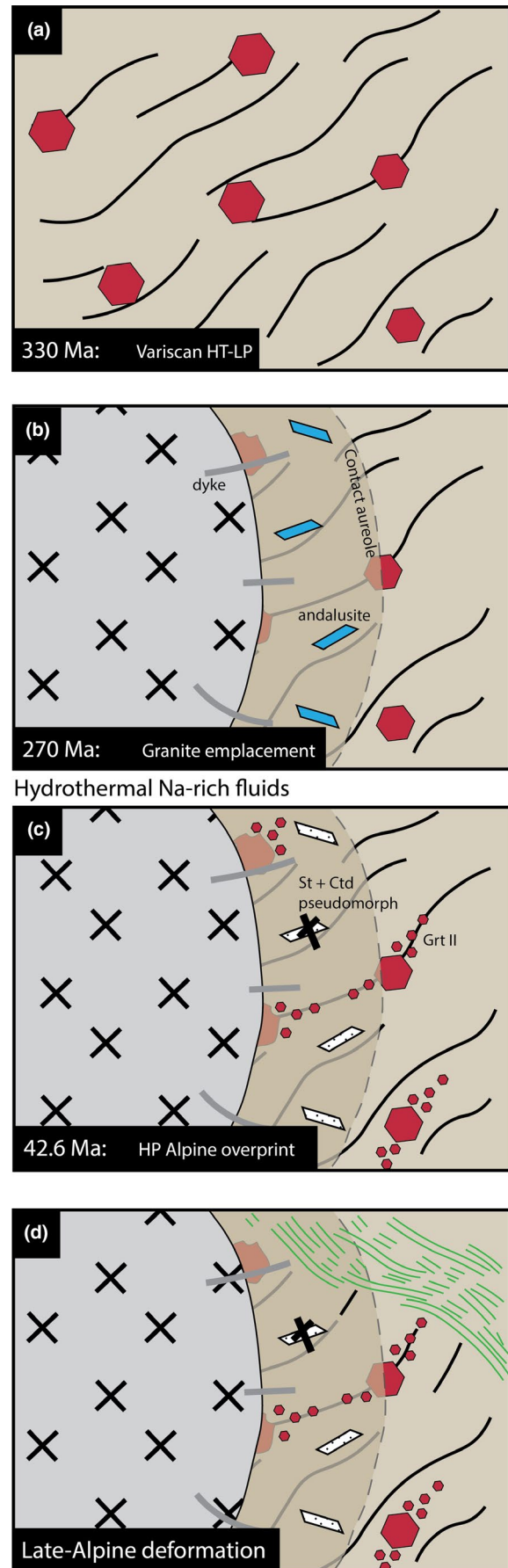
FIGURE 8 Schematic geological evolution of the polymetamorphic basement of Monte Rosa nappe: (a) Variscan high- T -low- P orogenic imprint, defined in this study as large first-generation garnet at 330 Ma (Engi et al., 2001), (b) intrusion of post-Variscan aged granite bodies (Pawlig & Baumgartner, 2001), associated dykes and associated contact metamorphic aureole most likely forming andalusite grade contact metapelites and late magmatic overprint by Na-saturated hydrothermal alteration, (c) HP imprint during Alpine orogenesis pseudomorphing after andalusite, forming the assemblages investigated in this study, (d) late Alpine deformation associated with decompression to greenschist facies grade

component in staurolite is important (Tuisku et al., 1987). The approach presented here is a suitable way of dealing with Zn-staurolite in the absence of experimentally constrained end-member thermodynamic data and where staurolite is the only Zn-bearing phase. The two model calculations (ideal molecular and site mixing) give reasonable bounds on the effect of Zn on the staurolite stability. Although not correlated with Zn content, Li-bearing staurolites have also been demonstrated to expand its stability field (e.g. Dutrow et al., 1986). However, we have not analysed Li in staurolite.

Concerning caveat (ii), one result from the calculations for assemblages 1 and 3 (Figure 7a–c) is the presence of quartz predicted in the stability field. Quartz modal abundance ranges from 1.0% to 0.1% with increasing pressure, temperature, and Si content of phengite (Figure 7a,b). However, after detailed microscope investigations and microprobe analysis of several pseudomorph domains from different samples we have not observed quartz associated with chloritoid and staurolite assemblages. This could be due to the very low proportions of quartz predicted (<1%) and the statistical chances of cutting a sample in order to observe quartz. Most likely there are two explanations for the predicted quartz: (1) white mica is an abundant phase and the K–Na exchange mixing model may be unreliable, thus Si in paragonite may not be accounted for, and (2) the garnet-bearing assemblages surrounding the pseudomorphs containing staurolite + chloritoid are observed to have quartz (Figure 5a,b), hence staurolite + chloritoid assemblages are most likely quartz saturated (or approaching quartz saturation).

7.3 | Tectono-metamorphic history of the metapelite

Figure 8 outlines the schematic geological history recorded in the metapelitic lithologies of the Monte Rosa. (a) Variscan HT–LP orogenesis, overprinting metapelitic lithologies, and the formation of first-generation garnet. (b) Intrusion of Variscan-age granite bodies, resulting in local migmatization and a contact metamorphic aureole forming andalusite. (c) Peak Alpine high- P imprint over contact metamorphic



andalusite resulting in staurolite–chloritoid within former andalusite pseudomorphs, and second-generation garnet-bearing assemblages. (d) Late Alpine deformation of the basement locally producing greenschist lithologies.

7.4 | Pressure variations and geodynamic implications

Figure 9a shows a comparison of the results of this study with the results from Luisier et al. (2019). When comparing the peak metamorphic conditions of metapelites from this study at 1.6 ± 0.2 GPa, with the peak metamorphic conditions of the whiteschist at 2.2 ± 0.2 GPa and the host metagranite at 1.4 ± 0.2 GPa, the metapelite and metagranite show a consistent peak pressure, within error, while the whiteschist shows a considerably higher peak P . Even with a conservative estimate (including the error range introduced via Zn-staurolite reduced activity), differences in peak pressure between metapelite and whiteschist are $\sim 0.6 \pm 0.2$ GPa. Peak temperature of approximately 550–600°C for the metagranite was estimated by Luisier et al. (2019) from the whiteschist pseudosection results. Assuming that the staurolite is a reliable thermometer (see staurolite-in line of Figure 5a), we are able to adjust the metagranite peak temperature estimates of Luisier et al. (2019) to our calculated temperatures of $585 \pm 20^\circ\text{C}$. Consequently, the data indicate that metagranite, metapelite, and whiteschist assemblages exhibit the same peak temperature, within error (Luisier et al., 2019).

There are two end-member interpretations for the geodynamic evolution of the Monte Rosa nappe, namely an interpretation based on lithostatic pressure (Figure 9b) and one based on tectonic pressure variations (Figure 9c). For the lithostatic interpretation, the peak pressure of the whiteschist

indicates a burial depth of the Monte Rosa nappe of ~ 80 km (using 2.35 GPa as peak pressure and assuming an overburden with an average density of $3,000 \text{ kg/m}^3$). Consequently, all peak pressure estimates for the metagranite and metapelite must be considered as totally unreliable, because all lithologies were at approximately the same burial depth (no tectonic mélange; see Section 2.3). In this scenario, the Monte Rosa nappe would have been most likely exhumed exclusively due to buoyancy forces (e.g. Butler et al., 2013, 2014).

We do not favour the lithostatic interpretation, because peak pressure estimates for metagranite and metapelite are consistent, within error, although the mineral assemblages are considerably different (Figure 9a). Also, the peak temperature estimates coincide with estimates for the whiteschist. Moreover, a characteristic structural feature of rocks exhumed by buoyancy in a subduction channel, under approximately lithostatic conditions, should be the formation of a tectonic mélange whereby rocks from different depths, having different peak pressure and temperature, are mixed inside the same tectonic units (Gerya & Stöckhert, 2006; Roda et al., 2012); but the studied region is not a mélange. For the tectonic pressure interpretation, peak pressure of the metagranite and metapelite indicate regional peak pressure of the Monte Rosa nappe whereas the peak pressure of the whiteschist indicates local pressure variations with pressures higher than the corresponding lithostatic value. Mechanically, such locally higher pressures could be due to compressional stress during the continental collision of the Alpine orogeny, or due to reaction-induced stresses due to volume changes during whiteschist formation (e.g. Luisier et al., 2019). We suggest that the higher pressure in the whiteschist was due to a combination of compressional and reaction-induced stresses. The ~ 1.6 Gpa peak pressure of the entire Monte Rosa nappe is compatible with the orogenic

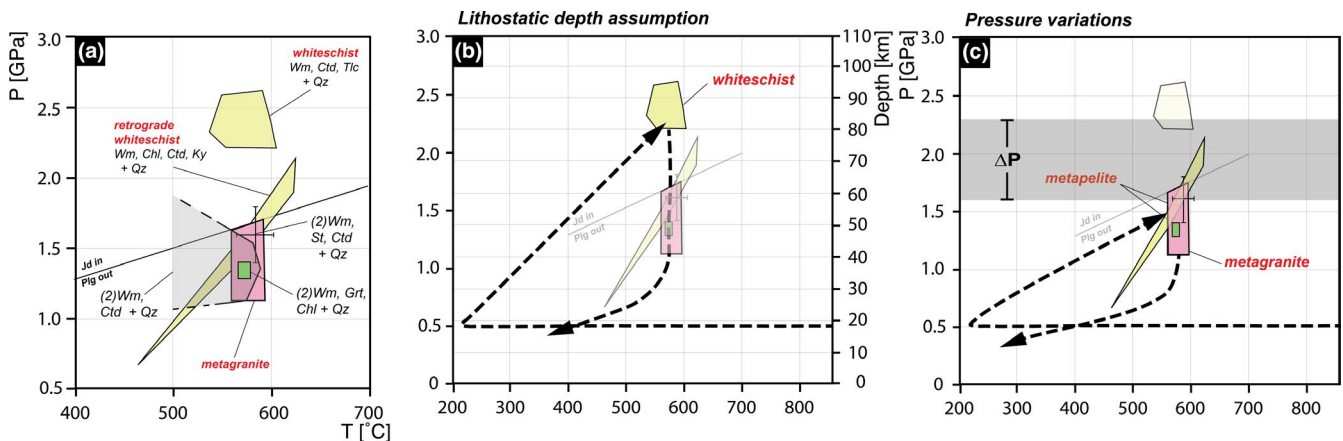


FIGURE 9 (a) Final PT results of metapelite samples and comparison of results with whiteschist assemblages and metagranite of Luisier et al. (2019); (b) hypothetical clockwise P – T –depth loop for the Monte Rosa nappe, peak pressure equating to deepest burial of unit using the lithostatic depth assumption, (c) hypothetical clockwise P – T loop for the Monte Rosa nappe where the metagranite and metapelites represent the regional peak pressure in the nappe and the whiteschist represents a local and volumetrically minor area of relatively higher pressure ΔP , potentially caused by mechanical- or reaction-induced stress

wedge model in which nappe stacking is due to a combination of buoyancy and compressive forces involving accretion, or underplating, during progressive subduction of mainly the European lower crust and mantle (e.g. Escher & Beaumont, 1997; Platt, 1986). Furthermore, Manzotti et al. (2018) recently estimated peak metamorphic conditions for the two main sub-units of the neighbouring Gran Paradiso massif (Figure 1), the Gran Paradiso and Money units, and dated the peak metamorphism. They obtained 1.8–2.0 Gpa and 500–520°C for the Gran Paradiso unit, and 1.7–1.8 Gpa and ~550°C for the Money unit; dated both at the same age of c. 42 Ma. The peak metamorphic conditions and age of the Gran Paradiso tectonic units are, hence, close to the peak metamorphic conditions of 1.6 ± 0.2 Gpa and $585 \pm 20^\circ\text{C}$ (and their age of 42.6 ± 0.6 Ma; Lapen et al., 2007), which are representative for the Monte Rosa nappe. We consider this similarity in peak metamorphic conditions of the two neighbouring internal crystalline massifs (Figure 1a) as further support for the feasibility of our proposed peak values.

8 | CONCLUSIONS


For the western portions of the Monte Rosa nappe, we have further constrained the metamorphic conditions associated with peak Alpine activity within the Western Alps from metapelitic lithologies. A unique staurolite–chloritoid-bearing assemblage was petrologically and thermodynamically investigated resulting in an Alpine peak pressure of 1.6 ± 0.2 GPa and a peak temperature of $585 \pm 20^\circ\text{C}$. Comparing these results with the peak pressure variations of 0.8 ± 0.3 GPa previously reported in metagranite lithologies, between whiteschist and metagranite, large peak pressure disparities of 0.6 ± 0.2 GPa persist (Figure 9). We rule out explanations for an apparent variability in pressure, such as sluggish kinetics in the metapelites or tectonic mixing, and further highlight the possible existence of mechanically and/or reaction-induced pressure differences.

Based on our new data and previously published results, we propose that the maximum burial depth of the Monte Rosa unit was likely significantly less than 80 km, which is a depth estimate based on the lithostatic pressure assumption and the local occurrence of minor volumes of whiteschist exhibiting peak pressure > 2.2 GPa. The maximum burial depth of the Monte Rosa unit was presumably less than 60 km, which is a depth compatible with burial and exhumation within an orogenic wedge. We further suggest that special care should be taken when using maximal values from published pressure estimates to reconstruct the burial and exhumation history of the corresponding tectonic unit, particularly, when the maximum pressure estimates are limited to minor volumes within the unit.

ACKNOWLEDGEMENTS

We thank B. Dutrow and an anonymous reviewer for their helpful and constructive reviews. This work was supported by the Swiss National Foundation grant numbers 200021-165756. J.V-H thanks Martin Robyr for assistance during EPMA data acquisition. J.V-H also thanks Evangelos Moulas for helpful discussions and guidance regarding thermodynamic adjustments.

ORCID

Joshua D. Vaughan-Hammon  <https://orcid.org/0000-0002-0388-146X>

REFERENCES

- Bearth, P. (1952). Geologie und petrographie des Monte Rosa. *Beitraege zur Geologischen Karte der Schweiz Lf.* 96, 1–94.
- Bearth, P. P. (1958). Über einen Wechsel der Mineralfazies in der Wurzelzone des Penninikums.
- Beltrando, M., Compagnoni, R., & Lombardo, B. (2010). (Ultra-) High-pressure metamorphism and orogenesis: An Alpine perspective. *Gondwana Research*, 18(1), 147–166.
- Berman, R. G. (1988). Internally-consistent thermodynamic data for minerals in the system $\text{Na}_2\text{O}-\text{K}_2\text{O}-\text{CaO}-\text{MgO}-\text{FeO}-\text{Fe}_2\text{O}_3-\text{Al}_2\text{O}_3-\text{SiO}_2-\text{TiO}_2-\text{H}_2\text{O}-\text{CO}_2$. *Journal of Petrology*, 29(2), 445–522.
- Berman, R. (1990). Mixing properties of Ca-Mg-Fe-Mn garnets. *American Mineralogist*, 75(3–4), 328–344.
- Borghi, A., Compagnoni, R., & Sandrone, R. (1996). Composite PT paths in the Internal Penninic Massifs of the Western Alps: Petrological constraints to their thermo-mechanical evolution.
- Butler, J. P., Beaumont, C., & Jamieson, R. A. (2013). The Alps 1: A working geodynamic model for burial and exhumation of (ultra) high-pressure rocks in Alpine-type orogens. *Earth and Planetary Science Letters*, 377, 114–131.
- Butler, J. P., Beaumont, C., & Jamieson, R. A. (2014). The Alps 2: Controls on crustal subduction and (ultra) high-pressure rock exhumation in Alpine-type orogens. *Journal of Geophysical Research: Solid Earth*, 119(7), 5987–6022.
- Chopin, C. (1987). Very-high-pressure metamorphism in the western Alps: Implications for subduction of continental crust. *Philosophical Transactions of the Royal Society of London. Series A, Mathematical and Physical Sciences*, 321(1557), 183–197.
- Chopin, C., Henry, C., & Michard, A. (1991). Geology and petrology of the coesite-bearing terrain, Dora Maira massif, Western Alps. *European Journal of Mineralogy*, 3(2), 263–291.
- Chopin, C., & Monié, P. (1984). A unique magnesiochloritoid-bearing, high-pressure assemblage from the Monte Rosa, Western Alps: Petrologic and 40 Ar-39 Ar radiometric study. *Contributions to Mineralogy and Petrology*, 87(4), 388–398.
- Dal Piaz, G. V. (2001). Geology of the Monte Rosa massif: Historical review and personal comments. *Schweizerische Mineralogische und Petrographische Mitteilungen*, 81(3), 275–303.
- Dal Piaz, G. V., & Lombardo, B. (1986). Early Alpine eclogite metamorphism in the Penninic Monte Rosa-Gran Paradiso basement nappes of the northwestern Alps. *Geological Society of America Memoir*, 164, 249–265.
- de Capitani, C., & Brown, T. H. (1987). The computation of chemical equilibrium in complex systems containing non-ideal solutions. *Geochimica et Cosmochimica Acta*, 51(10), 2639–2652.

- de Capitani, C., & Petrakakis, K. (2010). The computation of equilibrium assemblage diagrams with Theriak/Domino software. *American Mineralogist*, 95(7), 1006–1016.
- Deer, W., Howie, R., & Zussman, J. (2013). *An introduction to the rock-forming minerals*. London: Mineralogical Society of Great Britain and Ireland.
- Dutrow, B. L., Holdaway, M., & Hinton, R. (1986). Lithium in staurolite and its petrologic significance. *Contributions to Mineralogy and Petrology*, 94(4), 496–506.
- Ellis, D., & Green, D. (1979). An experimental study of the effect of Ca upon garnet-clinopyroxene Fe-Mg exchange equilibria. *Contributions to Mineralogy and Petrology*, 71(1), 13–22.
- Engi, M., Scherrer, N., & Burri, T. (2001). Metamorphic evolution of pelitic rocks of the Monte Rosa nappe. Constraints from petrology and single grain monazite age data. *Schweizerische Mineralogische und Petrographische Mitteilungen*, 81(3), 305–328.
- Escher, A., & Beaumont, C. (1997). Formation, burial and exhumation of basement nappes at crustal scale: A geometric model based on the Western Swiss-Italian Alps. *Journal of Structural Geology*, 19(7), 955–974.
- Eugster, H. P. (1985). Granites and hydrothermal ore deposits: A geochemical framework. *Mineralogical Magazine*, 49(350), 7–23.
- Ferrando, J., Scambelluri, M., Dal Piaz, G., & Piccardo, G. (2002). The mafic boudins of the southern Furgg-Zone, Monte Rosa nappe, NW-Italy: From tholeiitic continental basalts to Alpine eclogites and retrogressed products. 81 Riunione Estiva Soc. Geol. It., Torino: 10–12.
- Fox, J. (1971). Coexisting chloritoid and staurolite and the staurolite-chlorite isograd from the Agnew Lake area, Ontario. *Canada Geological Magazine*, 108(3), 205–219.
- Frey, M., Desmons, J., & Neubauer, F. (1999). Metamorphic maps of the Alps. Published by the editors and as enclosure to. *Schweizerische Mineralogische und Petrographische Mitteilungen*, 79(1).
- Gasco, I., Borghi, A., & Gattiglio, M. (2011). P-T Alpine metamorphic evolution of the Monte Rosa nappe along the Piedmont Zone boundary (Gressoney Valley, NW Italy). *Lithos*, 127(1–2), 336–353.
- Gerya, T. (2015). Tectonic overpressure and underpressure in lithospheric tectonics and metamorphism. *Journal of Metamorphic Geology*, 33(8), 785–800.
- Gerya, T., & Stöckhert, B. (2006). Two-dimensional numerical modeling of tectonic and metamorphic histories at active continental margins. *International Journal of Earth Sciences*, 95(2), 250–274.
- Goffe, B., & Chopin, C. (1986). High-pressure metamorphism in the Western Alps: Zoneography of metapelites, chronology and consequences. *Schweizerische Mineralogische und Petrographische Mitteilungen*, 66(1–2), 41–52.
- Griffen, D. T. (1981). Synthetic Fe/Zn staurolites and the ionic radius of $IVZn^{2+}$. *American Mineralogist*, 66(9–10), 932–937.
- Guidotti, C. V. (1970). The mineralogy and petrology of the transition from the lower to upper sillimanite zone in the Oquossoc area. *Maine. Journal of Petrology*, 11(2), 277–336.
- Hacker, B. R., & Gerya, T. V. (2013). Paradigms, new and old, for ultrahigh-pressure tectonism. *Tectonophysics*, 603, 79–88.
- Handy, M. R., Schmid, S. M., Bousquet, R., Kissling, E., & Bernoulli, D. (2010). Reconciling plate-tectonic reconstructions of Alpine Tethys with the geological-geophysical record of spreading and subduction in the Alps. *Earth-Science Reviews*, 102(3–4), 121–158.
- Hawthorne, F., Ungaretti, L., Oberti, R., Caucia, F., & Callegari, A. (1993). The crystal chemistry of staurolite; I, Crystal structure and site populations. *The Canadian Mineralogist*, 31(3), 551–582.
- Holdaway, M., Dutrow, B., & Shore, P. (1986). A model for the crystal chemistry of staurolite. *American Mineralogist*, 71(9–10), 1142–1159.
- Holdaway, M., Mukhopadhyay, B., Dyar, M. D., Dutrow, B. L., Rumble, D., & Grambling, J. A. (1991). A new perspective on staurolite crystal chemistry: Use of stoichiometric and chemical end-members for a mole fraction model. *American Mineralogist*, 76(11–12), 1910–1919.
- Holland, T. (1979). Reversed hydrothermal determination of jadeite-diopside activities. *Eos*, 60, 405.
- Holland, T., & Powell, R. (1998). An internally consistent thermodynamic data set for phases of petrological interest. *Journal of Metamorphic Geology*, 16(3), 309–343.
- Howie, R., Zussman, J., & Deer, W. (1992). *An introduction to the rock-forming minerals*. Longman.
- Huang, W., & Wyllie, P. (1974). Melting relations of muscovite with quartz and sanidine in the $K_2O-Al_2O_3-SiO_2-H_2O$ system to 30 kilobars and an outline of paragonite melting relations. *American Journal of Science*, 274(4), 378–395.
- Hurford, A. J., Hunziker, J. C., & Stöckhert, B. (1991). Constraints on the late thermotectonic evolution of the western Alps: Evidence for episodic rapid uplift. *Tectonics*, 10(4), 758–769.
- Kell, G., Haar, L., & Gallagher, J. (1984). NBS/NRC steam tables. Thermodynamic and transport properties and computer programs for vapor and liquid states of water in SI units. National Standard Reference Data.
- Keller, L., Abart, R., Stünitz, H., & De Capitani, C. (2004). Deformation, mass transfer and mineral reactions in an eclogite facies shear zone in a polymetamorphic metapelite (Monte Rosa nappe, western Alps). *Journal of Metamorphic Geology*, 22(2), 97–118.
- King, S. W. (1858). *The Italian Valleys of the Pennine Alps: A Tour Through All the Romantic and Less-frequented "vals" of Northern Piedmont, from the Tarentaise to the Gries*. J. Murray.
- Kurz, W., & Froitzheim, N. (2002). The exhumation of eclogite-facies metamorphic rocks – A review of models confronted with examples from the Alps. *International Geology Review*, 44(8), 702–743.
- Lanari, P., Vidal, O., De Andrade, V., Dubacq, B., Lewin, E., Grosch, E. G., & Schwartz, S. (2014). XMapTools: A MATLAB®-based program for electron microprobe X-ray image processing and geothermobarometry. *Computers & Geosciences*, 62, 227–240.
- Lapen, T. J., Johnson, C. M., Baumgartner, L. P., Dal Piaz, G. V., Skora, S., & Beard, B. L. (2007). Coupling of oceanic and continental crust during Eocene eclogite-facies metamorphism: Evidence from the Monte Rosa nappe, western Alps. *Contributions to Mineralogy and Petrology*, 153(2), 139–157.
- Le Bayon, R., de Capitani, C., & Frey, M. (2006). Modelling phase-assemblage diagrams for magnesian metapelites in the system $K_2O-FeO-MgO-Al_2O_3-SiO_2-H_2O$: Geodynamic consequences for the Monte Rosa nappe, Western Alps. *Contributions to Mineralogy and Petrology*, 151(4), 395.
- Li, Z. H., Gerya, T. V., & Burg, J.-P. (2010). Influence of tectonic overpressure on P-T paths of HP-UHP rocks in continental collision zones: Thermomechanical modelling. *Journal of Metamorphic Geology*, 28(3), 227–247.
- Luisier, C., Baumgartner, L., Schmalholz, S. M., Siron, G., & Vennemann, T. (2019). Metamorphic pressure variation in a coherent Alpine nappe challenges lithostatic pressure paradigm. *Nature Communications*, 10(1), 1–11.
- Mancktelow, N. (1993). Tectonic overpressure in competent mafic layers and the development of isolated eclogites. *Journal of Metamorphic Geology*, 11(6), 801–812.

- Mancktelow, N. S. (1995). Nonlithostatic pressure during sediment subduction and the development and exhumation of high pressure metamorphic rocks. *Journal of Geophysical Research: Solid Earth*, 100(B1), 571–583.
- Mancktelow, N. S. (2008). Tectonic pressure: Theoretical concepts and modelled examples. *Lithos*, 103(1–2), 149–177.
- Manzotti, P. et al (2018). Exhumation rates in the Gran Paradiso Massif (Western Alps) constrained by in situ U–Th–Pb dating of accessory phases (monazite, allanite and xenotime). *Contributions to Mineralogy and Petrology*, 173(3), 24.
- Marger, K., Luisier, C., Baumgartner, L., Putlitz, B., & Dutrow, B. (2019). Origin of Monte Rosa whiteschist from in-situ tourmaline and quartz oxygen isotope analysis by SIMS using new tourmaline reference materials. *American Mineralogist: Journal of Earth and Planetary Materials*, 104(10), 1503–1520.
- Massonne, H.-J., & Schreyer, W. (1987). Phengite geobarometry based on the limiting assemblage with K-feldspar, phlogopite, and quartz. *Contributions to Mineralogy and Petrology*, 96(2), 212–224.
- Massonne, H.-J., & Szpurka, Z. (1997). Thermodynamic properties of white micas on the basis of high-pressure experiments in the systems K_2O - MgO - Al_2O_3 - SiO_2 - H_2O and K_2O - FeO - Al_2O_3 - SiO_2 - H_2O . *Lithos*, 41(1–3), 229–250.
- Molnar, P., & Lyon-Caen, H. (1988). Some simple physical aspects of the support, structure, and evolution of mountain belts. *Processes in Continental Lithospheric Deformation*, 218, 179–207.
- Moulas, E., Schmalholz, S. M., Podladchikov, Y., Tajčmanová, L., Kostopoulos, D., & Baumgartner, L. (2019). Relation between mean stress, thermodynamic, and lithostatic pressure. *Journal of Metamorphic Geology*, 37(1), 1–14.
- Nagel, T., De Capitani, C., & Frey, M. (2002). Isograds and P–T evolution in the eastern Lepontine Alps (Graubünden, Switzerland). *Journal of Metamorphic Geology*, 20(3), 309–324.
- Niggli, E. (1960). Mineral-zonen der alpinen Metamorphose in den Schweizer Alpen. Int. geol. Congr. Copenhagen, Rep. 21st Sess. Norden, 13, 132–138.
- Niggli, E. (1970). *Alpine Metamorphose und Alpine Gebirgsbildung*. Fortschr. Miner.
- Niggli, E., & Niggli, C. (1965). Karten der Verbreitung einiger Mineralien der alpidischen Metamorphose in den Schweizer Alpen (Stilpnomelan, Alkali-Amphibol, Chloritoid, Staurolith, Disthen, Sillimanit). *Eclogae Geologicae Helveticae*, 58, 335–368.
- Pawlig, S. (2001). Geological evolution of the Monte Rosa: constraints from geochronology and geochemistry of a talc kyanite chloritoid shear zone within the Monte Rosa granite (Monte Rosa nappe, Italian Western Alps), Verlag nicht ermittelbar.
- Pawlig, S., & Baumgartner, L. (2001). Geochemistry of a talc-kyanite-chloritoid shear zone within the Monte Rosa granite, Val d'Ayas, Italy. *Schweizerische mineralogische und petrographische Mitteilungen*, 81, 329–346.
- Petrini, K., & Podladchikov, Y. (2000). Lithospheric pressure–depth relationship in compressive regions of thickened crust. *Journal of Metamorphic Geology*, 18, 67–77.
- Platt, J. (1986). Dynamics of orogenic wedges and the uplift of high-pressure metamorphic rocks. *Geological Society of America Bulletin*, 97(9), 1037–1053.
- Powell, R., & Holland, T. (1993). On the formulation of simple mixing models for complex phases. *American Mineralogist*, 78(11–12), 1174–1180.
- Rao, B., & Johannes, W. (1979). Further data on the stability of staurolite. *Neues Jahrb. Mineral. Monatsh*, 10, 437–447.
- Reinecke, T. (1991). Very-high-pressure metamorphism and uplift of coesite-bearing metasediments from the Zermatt-Saas zone, Western Alps. *European Journal of Mineralogy*, 7–18.
- Reuber, G., Kaus, B. J., Schmalholz, S. M., & White, R. W. (2016). Nonlithostatic pressure during subduction and collision and the formation of (ultra) high-pressure rocks. *Geology*, 44(5), 343–346.
- Roda, M., Spalla, M. I., & Marotta, A. M. (2012). Integration of natural data within a numerical model of ablative subduction: A possible interpretation for the Alpine dynamics of the Austroalpine crust. *Journal of Metamorphic Geology*, 30(9), 973–996.
- Schenker, F. L., Schmalholz, S. M., Moulas, E., Pleuger, J., Baumgartner, L. P., Podladchikov, Y., Vrijmoed, J., Buchs, N., & Müntener, O. (2015). Current challenges for explaining (ultra) high-pressure tectonism in the Pennine domain of the Central and Western Alps. *Journal of Metamorphic Geology*, 33(8), 869–886.
- Schmalholz, S. M., Duretz, T., Hetényi, G., & Medvedev, S. (2019). Distribution and magnitude of stress due to lateral variation of gravitational potential energy between Indian lowland and Tibetan plateau. *Geophysical Journal International*, 216(2), 1313–1333.
- Schmalholz, S. M., Medvedev, S., Lechmann, S. M., & Podladchikov, Y. (2014). Relationship between tectonic overpressure, deviatoric stress, driving force, isostasy and gravitational potential energy. *Geophysical Journal International*, 197(2), 680–696.
- Schmalholz, S. M., & Podladchikov, Y. Y. (2013). Tectonic overpressure in weak crustal-scale shear zones and implications for the exhumation of high-pressure rocks. *Geophysical Research Letters*, 40(10), 1984–1988.
- Schmalholz, S. M., & Podladchikov, Y. (2014). Metamorphism under stress: The problem of relating minerals to depth. *Geology*, 42(8), 733–734.
- Skora, S., Mahlen, N. J., Johnson, C. M., Baumgartner, L. P., Lapen, T. J., Beard, B. L., & Szilvagy, E. T. (2015). Evidence for protracted prograde metamorphism followed by rapid exhumation of the Zermatt-Saas Fee ophiolite. *Journal of Metamorphic Geology*, 33(7), 711–734.
- Steck, A., Masson, H., & Robyr, M. (2015). Tectonics of the Monte Rosa and surrounding nappes (Switzerland and Italy): Tertiary phases of subduction, thrusting and folding in the Pennine Alps. *Swiss Journal of Geosciences*, 108(1), 3–34.
- Tuisku, P., Ruosresuo, P., & Häkkinen, A.-M. (1987). The metamorphic behaviour and petrogenetic significance of zinc in amphibolite facies, staurolite-bearing mica schists, Puolankajärvi Formation. *Central Finland. Geochimica et Cosmochimica Acta*, 51(6), 1639–1650.
- Wheeler, J. (2018). The effects of stress on reactions in the Earth: Sometimes rather mean, usually normal, always important. *Journal of Metamorphic Geology*, 36(4), 439–461.
- Whitney, D. L., & Evans, B. W. (2010). Abbreviations for names of rock-forming minerals. *American Mineralogist*, 95(1), 185–187. <https://doi.org/10.2138/am.2010.3371>

SUPPORTING INFORMATION

Additional supporting information may be found online in the Supporting Information section.

FIGURE S1. Field image of typical migmatitic textures in the Monte Rosa metapelites in close proximity to metagranite bodies

FIGURE S2. Field image of late Alpine folding in the metapelitic basement. Preserving early Alpine assemblages

in the fold hinge.

FIGURE S3. Field image of earl Alpine high-*P* assemblages pseudomorphing contact metamorphic textures

FIGURE S4. Mineralogical and textural overview of samples 16MR-17.

FIGURE S5. Xray cps. map of first-generation garnet in samples 16MR-17.

FIGURE S6. SEM image of assemblage 1.

FIGURE S7. Phase proportion map generated via XMapTools for assemblage 1 of 16MR-17.

FIGURE S8. Mg versus Fe total (a.p.f.u.) for chloritoid in assemblage 1.

FIGURE S9. Estimated Mg²⁺ versus Fe²⁺ (a.p.f.u.) for chloritoid in assemblage 1.

FIGURE S10. Ca, Fe², Mg, and Mn profiles in second-generation garnet of assemblage 2 from samples 16MR-17.

FIGURE S11. Phase proportion map generated via XMapTools for assemblage 2 of 16MR-17.

APPENDIX S1. Field observations and chemical data

How to cite this article: Vaughan-Hammon JD, Luisier C, Baumgartner LP, Schmalholz SM. Peak Alpine metamorphic conditions from staurolite-bearing metapelites in the Monte Rosa nappe (Central European Alps) and geodynamic implications. *J Metamorph Geol.* 2021;00:1–21. <https://doi.org/10.1111/jmg.12595>

APPENDIX 1

FE AND MG END-MEMBER CORRECTIONS FOR ZN IN STAULOLITE

Due to the absence of thermodynamic data for Zn-staurolite end-members (Fox, 1971; Holdaway et al., 1986, 1991), the experimentally derived thermodynamic activity of available end-members (i.e. Fe- or Mg-staurolite) must be adjusted. In order to adjust the activity for end-members for non-negligible Zn values we begin with the general equation of the apparent Gibbs free energy (*G*) for a single component defined in Theriak/Domino (de Capitani & Petrakakis, 2010):

$$G_i^{T,P} = H_i^{T_0,P_0} - TS_i^{T_0,P_0} + \int_{T_0}^T Cp_i dT - T \int_{T_0}^T \frac{Cp_i}{T} dT + \int_{P_0}^P V_i^{T,P_0} dP \quad (1.1)$$

For a single mineral end-member the index *i* = 1. In the case of a multi-component ideal solution, *G*_{sol} would equal:

$$G_{\text{sol}} = G^{\text{mech}} + G^{\text{mix}} = \sum_{i=1}^n x_i G_i + \sum_{i=1}^n x_i RT \ln(\alpha_i^{\text{ideal}}) \quad (1.2)$$

The *x_i* represent the relative fraction of each component and $\sum_{i=1}^n x_i = 1$. The Gibbs energy for the single component of Mg-staurolite (MgSt) is:

$$G_{\text{MgSt}}^{T,P} = H_{\text{MgSt}}^{T_0,P_0} - TS_{\text{MgSt}}^{T_0,P_0} + \int_{T_0}^T Cp_{\text{MgSt}} dT - T \int_{T_0}^T \frac{Cp_{\text{MgSt}}}{T} dT + \int_{P_0}^P V_{\text{MgSt}}^{T,P_0} dP \quad (1.3)$$

The end-member adjustment for a single component (e.g. MgSt & *x_i* = 1) is performed by modifying *S*_{MgSt}^{T₀,P₀} in Equation (1.3). For reducing the activity of the pure (*x_i* ≈ 1) end-member (e.g. MgSt) and due to the presence of Zn (Zn-MgSt) we introduce the mixing term (*G*^{mix} in Equation (1.2)) in Equation (1.3) and assume that the remaining thermodynamic properties of the Zn-bearing MgSt are identical:

$$G_{\text{Zn-MgSt}}^{T,P} \approx H_{\text{MgSt}}^{T_0,P_0} - TS_{\text{MgSt}}^{T_0,P_0} + \int_{T_0}^T Cp_{\text{MgSt}} dT - T \int_{T_0}^T \frac{Cp_{\text{MgSt}}}{T} dT + \int_{P_0}^P V_{\text{MgSt}}^{T,P_0} dP + RT \ln(\alpha_i^{\text{reduced}}) \quad (1.4)$$

For pure St end-members (Zn free), Equations (1.4) and (1.3) are equivalent because $\alpha_i^{\text{reduced}} = 1$. Instead of explicitly treating the mixing term in the Gibbs energy Equation (1.4) we prefer to introduce an ‘effective’ entropy (*S*_{eff}^{T₀,P₀}) in the Gibbs equation, which includes the mixing term. We thus write:

$$G_{\text{Zn-MgSt}}^{T,P} \approx H_{\text{MgSt}}^{T_0,P_0} - TS_{\text{eff}}^{T_0,P_0} + \int_{T_0}^T Cp_{\text{MgSt}} dT - T \int_{T_0}^T \frac{Cp_{\text{MgSt}}}{T} dT + \int_{P_0}^P V_{\text{MgSt}}^{T,P_0} dP \quad (1.5)$$

Equations (1.4) and (1.5) must be equivalent expressions and their difference must, hence, be zero. Subtracting Equations (1.4) and (1.5) yields:

$$-TS_{\text{eff}}^{T_0,P_0} + TS_{\text{MgSt}}^{T_0,P_0} - RT \ln(\alpha_i^{\text{reduced}}) = 0 \quad (1.6)$$

which after division by temperature and rearrangement provides the expression for the ‘effective’ entropy:

$$S_{\text{eff}}^{T_0,P_0} = S_{\text{MgSt}}^{T_0,P_0} - R \ln(\alpha_i^{\text{reduced}}) \quad (1.7)$$

Therefore, the presence of Zn, causing $\alpha_i^{\text{reduced}} < 1$, would always increase the total entropy via *S*_{eff}^{T₀,P₀} and therefore reduce the *G*^{T,P} of the mixture.

We do not adjust H^0 (Fe-staurolite = -23765364 J/mol and Mg-staurolite = -25112909 J/mol) within THERIAK-DOMINO after Nagel et al. (2002). $S_{\text{eff}}^{T_0, P_0}$ defines an entropy correction, where $S_{\text{MgSt}}^{T_0, P_0}$ is the entropy for the pure phase after Nagel et al. (2002; Fe-staurolite = $1,005.327$ J·mol $^{-1}$ ·K $^{-1}$ and Mg-staurolite 905.396 J mol $^{-1}$ K $^{-1}$). For a pure phase, $\alpha_i^{\text{reduced}} = 1$, thus $S_{\text{eff}}^{T_0, P_0} = S_{\text{MgSt}}^{T_0, P_0}$. Due to the site multiplicity of staurolite being 4 (T2, M1–M4) and the equivalent substitutions being Fe $^{2+}$ = Mg = Zn (e.g. Holdaway et al., 1986) we are able to calculate two potential ‘end-member’ mixing models in order to correct the activity of Mg and Fe end-members. Firstly, a ‘molecular mixing’ model that

assumes components are equivalent to mole fractions, thus a linear mixing model via $\alpha_i^{\text{reduced}} = \left(1 - \left(\frac{Zn}{4}\right)\right)$. Where Zn = 0.99 atoms per formula unit (a.p.f.u.; Table 1), the resulting $S_{\text{eff}}^{T_0, P_0}$ for Fe-staurolite is $1,007.6911$ J mol $^{-1}$ K $^{-1}$ and Mg-staurolite 907.7601 J mol $^{-1}$ K $^{-1}$. The second, ‘site mixing’ model has a dependence on the site multiplicity of staurolite being 4 (Holdaway et al., 1991), thus a highly non-linear dependence via $\alpha_i^{\text{reduced}} = \left(1 - \left(\frac{Zn}{4}\right)\right)^4$. Where Zn = 0.99 a.p.f.u. (Table 1), the resulting $S_{\text{eff}}^{T_0, P_0}$ for Fe-staurolite is $1,014.7834$ J mol $^{-1}$ K $^{-1}$ and Mg-staurolite 914.8524 J mol $^{-1}$ K $^{-1}$.